



CHALMERS
UNIVERSITY OF TECHNOLOGY

Instrumented Safety Device for Osseointegrated Transfemoral Prostheses

Master's thesis in Biomedical Engineering

HÖGNA HRINGSDÓTTIR

MASTER'S THESIS IN BIOMEDICAL ENGINEERING

Instrumented Safety Device for Osseointegrated Transfemoral Prostheses

HÖGNA HRINGSDÓTTIR

Department of Signals and Systems
Division of Signal Processing and Biomedical Engineering
CHALMERS UNIVERSITY OF TECHNOLOGY
Göteborg, Sweden 2016

Instrumented Safety Device for Osseointegrated Transfemoral Prostheses

HÖGNA HRINGSDÓTTIR

© HÖGNA HRINGSDÓTTIR, 2016-06-07

Master's Thesis EX015/2016
Department of Signals and Systems
Division of Signal Processing and Biomedical Engineering
Chalmers University of Technology
SE-412 96 Göteborg
Sweden

Department of Signals and Systems
Göteborg, Sweden 2016-06-07

Abstract

The Osseointegrated Prostheses for the Rehabilitation of Amputees (OPRA) Implant System is a bone anchoring method where osseointegration plays a key role, allowing the prosthesis to be directly attached to the bone. To date, limited amount of information is available on peak moments and stresses during activities of the daily living. This information can be crucial for identification of potential failure modes, improvement of implant design and optimization of a rehabilitation program. The objective of this project was therefore to instrument a prosthetic coupling device which would be embedded with monitoring capabilities.

The Axor™ II is a safety device commonly used with the OPRA Implant System to protect the implant from high moments through a release mechanism. This device was equipped with an acquisition system, by instrumenting it with strain gauges, along with the necessary electronics, algorithms and communication modules, in order to obtain a functional prototype. The acquisition system was prototyped using a low cost microcontroller (TIVA, Texas Instruments), and was made accessible via a custom designed graphical user interface in Matlab for configuration and data retrieval. Two communication modules were designed: one for real time communication, where the data gets sent directly to the Universal Asynchronous Receiver-Transmitter, and one for SD (Secure Digital) card communication, where the data gets saved to an SD card.

Once the communication aspects were solved, several tests were conducted to verify functionality and reliability. It was found that the axial force could not be measured from the selected location of the strain gauges. Torsional moments were challenging due to friction and/or an apparent latching during directional changes that induced a steady shift of the baseline. The results for the measured bending moments were reliable and found similar to those obtained with a commercially available 6-axis transducer.

The obtained results imply that the axial force/torque applied to the device does not fully transfer to the part inside the Axor where the strain gauges were mounted. Consequently, the selected placement of the strain gauges for axial force and torque needs to be revised. Bending moments were successfully recorded in a patient during ambulation, which verified the functionality of the designed electronics and acquisition algorithms. While this work has demonstrated the feasibility of the concept, further work is necessary before this technology can be used in activities of the daily living.

Key words: osseointegration, OPRA Implant System, Axor, abutment, transducer, instrumentation, strain gauges, PCB, acquisition system, communication modules, Tiva Launchpad, Matlab GUI, UART, axial force, bending moments, torsional moments, baseline shift.

Acknowledgement

First, I would like to thank my supervisor Max Ortiz Catalan for his guidance and unconditional support throughout the whole project. My sincere thanks go to Enzo Mastinu, Marta Björnsdóttir and Jason Millenaar at Integrum for being there when I needed to reflect ideas or problems, and their assistance during the course of this thesis. Also, special thanks go to Katarzyna Kulbacka-Ortiz for her assistance in obtaining ethical approval. Finally, I would like to thank my examiner Sabine Reinfeldt for her valuable comments and support with the thesis writing.

Contents

Abstract	I
Acknowledgement.....	II
Contents	III
Abbreviations and Acronyms	V
1 Introduction.....	1
1.1 Suspension Methods	1
1.2 Osseointegration.....	2
1.3 OPRA Implant System.....	2
1.4 Aim of Thesis	5
2 State of the Art Load Monitoring Systems.....	6
2.1 Gait Laboratories.....	6
2.2 Portable Monitoring Systems.....	6
3 Theory.....	10
3.1 Strain Gauges.....	10
3.2 The Measurement System	11
3.3 Wheatstone Bridge Configuration.....	12
3.4 Offset Nulling.....	16
3.5 Unit conversion.....	16
4 Previous Work	18
4.1 Selection of Strain Gauges.....	18
4.2 Placement of Strain Gauges and Signal Conditioning.....	19
5 Methodology	21
5.1 System Requirements	21
5.2 Repairing of Current device	21
5.2.1 PCB	21
5.2.2 Strain Gauges.....	22
5.3 Firmware.....	23
5.3.1 ADC Acquisition.....	23
5.3.2 PC Interface.....	26
5.4 Unit Conversion.....	27
5.5 Offset Nulling.....	28
5.6 Instrumentation Amplifiers - Determining the Gain	28
5.7 Testing	29

5.7.1	Selecting Appropriate Gain Resistances.....	29
5.7.2	Calibration Test.....	32
5.7.3	Comparison Test.....	32
5.7.4	SD Card Communication.....	34
5.8	External Battery.....	36
5.9	Housing for the Electronics.....	36
5.10	Patient Pilot.....	37
6	Results.....	39
6.1	Unit Conversion.....	39
6.2	Testing.....	39
6.2.1	Selecting Appropriate Gain Resistances.....	39
6.2.2	Calibration Test.....	40
6.2.3	Comparison Test.....	42
6.2.4	SD Card Communication.....	46
6.3	Patient Pilot.....	46
7	Discussion.....	49
7.1	Testing.....	49
7.1.1	Selecting Appropriate Gain Resistances.....	49
7.1.2	Calibration Test.....	49
7.1.3	Comparison Test.....	50
7.1.4	SD Card Communication.....	51
7.2	Patient Pilot.....	51
7.3	Updated design.....	52
7.4	Future Work.....	53
8	Conclusion.....	55
9	References.....	56

Abbreviations and Acronyms

ADC	Analog to Digital Conversion
AP	Anteroposterior
FS	Floor Sensors
FSRs	Force Sensitive Resistors
GPIO	General Purpose Input/Output
GPS	Global Positioning System
IDE	Integrated Development Environment
IP	Image Processing
MCU	Microcontroller Unit
ML	Mediolateral
NWS	Non-wearable Sensors
OPRA	Osseointegrated Prostheses for the Rehabilitation of Amputees
PCB	Printed Circuit Board
PVDF	Polyvinylidene Fluoride
ROM	Range of Motion
SD	Secure Digital
UART	Universal Asynchronous Receiver-Transmitter
WS	Wearable Sensors

A	Cross sectional area
D	Outer diameter
d	Inner diameter
dR	Change in resistance due to strain
e	Strain
E	Young's modulus of elasticity
F_A	Axial load
G	Shear modulus
M_B	Bending moment
M_T	Torsional moment
R	Strain gauge resistance before deformation
R_G	Gain resistance
$R_{x(x=1,2,3,4)}$	Bridge resistance
S	Sectional modulus
S_e	Gauge factor
S_p	Polar section modulus
V_{Ex}	Excitation voltage
V_o	Output voltage
σ	Direct stress
τ	Shear stress

1 Introduction

Amputation is defined as the surgical removal of a limb and in the year 2007 around 1.7 million people were living with limb loss in the United States alone. The causes for amputation can vary, but the main ones are: circulatory diseases (70%), trauma (23%), tumors (4%), and congenital conditions (3%). [1] Prosthetic technology has progressed rapidly in recent years with new inventions that have greatly improved the quality of life for amputees. Although the design of the prostheses is important in terms of comfort for the patient, the interface between the body and the artificial limb is just as critical. Therefore, this aspect must also be focused on in prosthetic design.

1.1 Suspension Methods

In prosthetics there are two main suspension methods, namely **the conventional socket system** and **the bone-anchored prosthesis system**. The conventional socket system is the most common suspension system and consists of a **hard socket**, which is used to suspend the artificial limb, and a **liner**, which covers the stump of the patient, see Figure 1. The connection between the liner and the socket can vary, but the main ones are **vacuum assisted** or **mechanical** (such as a pin-lock suspension system). [2][3]

Although conventional socket systems have proven to be very beneficial for many patients, they do have downsides where the most frequently reported problems are related to sore/skin irritation, tissue breakdown and general limb pain due to the friction on the stump/socket interface. Another disadvantage relates to heat/sweating inside the socket on account of the skins inability to breathe. Furthermore, the socket considerably limits the range of motion (ROM) of the residual limb and can cause discomfort when wearing the prosthesis. [4][5][6]

With the other attachment method, the bone-anchored prosthesis system, the artificial limb is attached directly to the skeleton through what is known as osseointegration. This approach excludes the need of a prosthetic socket and has shown to improve the quality of life for users who previously had problems with a prosthetic socket fit. [7]

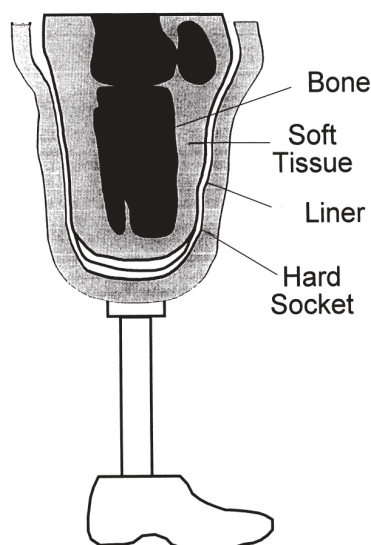


Figure 1: Components of a conventional socket system [2].

1.2 Osseointegration

“Osseointegration was originally defined as a direct structural and functional connection between ordered living bone and the surface of a load-carrying implant” (Branemårk *et al.*, 2001, p. 176). Now, however, implants are considered osseointegrated when there is no movement between the implant itself and the bone tissue it is in direct contact with. Osseointegration was discovered by Professor Per-Ingvar Brånemark in the early 1950s by accident during an experiment performed on rabbits. In the study, titanium implant chambers were threaded into rabbit bone to analyze the blood flow in the bone. When the titanium implants were to be removed at the end of the experiment, the rabbit bone had fully integrated with the implant thus making it difficult to disengage. This discovery together with the fact that titanium was not rejected by the body was groundbreaking and the beginning of an extensive clinical research in the field of osseointegration. [8]

To begin with, the discovery was used in the dental industry where osseointegrated implants were used to support prosthetic tooth replacements, but since then it has further progressed. To date, osseointegration plays also a key role in applications such as bone anchored limb prostheses, bone anchored hearing aids, knee and joint replacements, and facial prosthetics, to name a few. [7] This thesis will however mainly focus on osseointegrated transfemoral amputation prostheses.

1.3 OPRA Implant System

Treatment with osseointegrated transfemoral prostheses, where the prosthesis is directly anchored to the bone, has proven to be very beneficial for amputees, and has been performed in Sweden since 1990. To begin with, the rehabilitation process was not standardized which resulted in some treatment failures, but in 1999 a treatment protocol called **Osseointegrated Prostheses for the Rehabilitation of Amputees (OPRA)**, was established. The OPRA protocol includes two surgical procedures where the OPRA Implant System (Integrum AB, Sweden), consisting of a fixture, an abutment and an abutment screw, is implanted into the patient, see Figure 2. In the first procedure a titanium fixture is inserted into the residual femur and then the skin closed for healing. To make sure the implant integrates with the bone, it is important that the fixture is left unloaded while the distal scar is healing. The second surgery is performed 6 months after the first surgery. This procedure consists of a skin and soft tissue penetration, to allow for the abutment to be inserted into the distal end of the fixture, see Figure 3. After the second surgery, the patient must be immobilized for at least 10-12 days to ensure critical healing of the soft tissue and skin area around the penetrating abutment. [7][9]

Even though the osseointegration process starts during the first 6 months (the interval between surgeries), the bone tissue covering the implant requires controlled loading of the implant to further enhance the bone strength after the second surgery. Six weeks following the second surgery, the patient is fitted with a training prosthesis which allows him/her to load the implant. The load applied to the implant should increase gradually every week with the aim of preparing for the use of the artificial limb. The rehabilitation process needs to be thoroughly followed, since rapid increase in implant loading can result in implant loosening. The patient should be able to apply full body weight to the prosthesis without experiencing pain two or three months after the second surgery, which then enables him/her to be fitted with a prosthesis meant for daily use. [7][9][10]

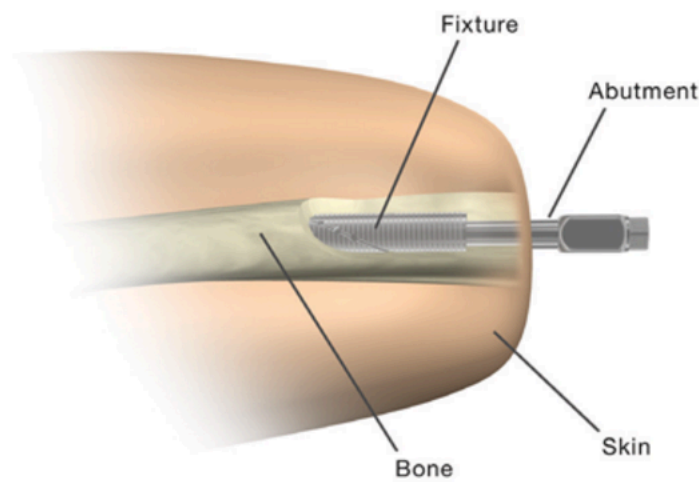


Figure 2: OPRA Implant System (Integrum AB, Sweden) implanted in a transfemoral amputee [11].



Figure 3: The residual limb of a transfemoral amputee fitted with the OPRA Implant System [7].

The OPRA Implant System has played a crucial role in improving patient's quality of life compared to the conventional socket system. The system provides increased range of motion, it eliminates sore/skin irritation, tissue breakdown and pain caused by the stump/socket interface, it provides osseoperception¹, provides better walking ability, improves sitting comfort, and most of all, it is suitable for very short stumps that can not be fitted with conventional socket systems. [11][12] Although the system has proven beneficial, there are downsides that need to be considered. The main disadvantages are related to the long rehabilitation time, the risk of infection around the abutment area, the risk of bone fractures and implant loosening, and the fact that high-impact activities are not recommended (e.g. jumping, running etc.).

The reason why high-impact activities should be avoided is due to the fact that bone is mechanically weaker than titanium, and can potentially break before the titanium implant, should the OPRA Implant System be exposed to excessive loads. This risk is addressed in two ways. First, the OPRA implant is designed by the weakest link concept. The weakest part is the abutment screw, which is also the part which is the easiest to replace. The abutment is the second weakest part where the replacement procedure is also more invasive. The fixture is the strongest and should not fail. The second safety measure is a mechanical safety device designed to be used as a part of the OPRA Implant System. The safety device is called the OPRA Axor™ II (hereafter called Axor), see Figure 4. The Axor is designed to protect the system from high moments, by limiting them from being transferred to the implant. This is done by utilizing two release mechanisms, i.e. a bend and rotation release mechanisms. Even though the safety device plays a crucial role in preventing implant failures, caution needs to be taken and high-impact activities should still be avoided. [13]

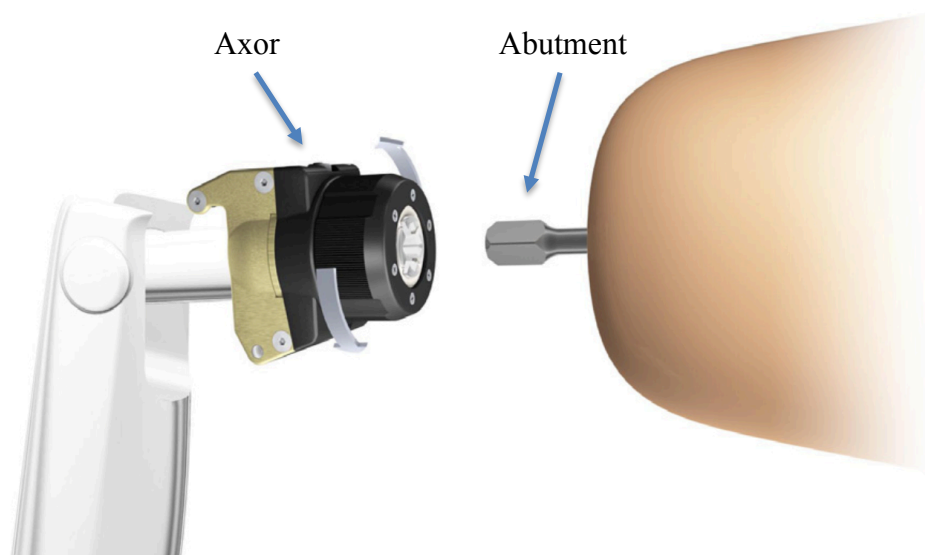


Figure 4: Connecting the abutment (right) to the Axor (left) [13].

¹ “Osseoperception is the term given to the patient-reported with feeling of heightened perception of the environment with osseointegrated prostheses.” (Kumar *et al.*, 2012, p. 1)

To date, limited information is available on the loading scenario during daily use of the OPRA Implant System. This information could possibly be used to inform on potential failure modes and prevent service actions to the implant system, since components (such as the abutment) could be changed before breakage. In addition, the gathered information is vital for further implant development and optimization of rehabilitation and exercise programs. Although commercially available load cells could be utilized in order to obtain this information, they are limiting due to high costs and the added build height to the prosthesis, thus excluding users with long stumps. Also, for the Axor to work properly, the load cells would have to be positioned between the Axor and the prosthetic knee thus creating potential safety concerns and additive errors.

1.4 Aim of Thesis

The aim of this thesis is to instrument a prosthetic coupling device which will be embedded with monitoring capabilities. This is achieved by redesigning the Axor such that a monitoring feature can be added to the device, without adding build height to the prosthesis, and at the same time minimize the error in the load monitoring process (compared to commercially available load cells). The redesigned Axor is consequently being upgraded from mechanics to mechatronics. In order to implement this, the Axor is instrumented with strain gauges. The selection and location of strain gauges has been determined in previous work, see section 4 [14]. This thesis extends on this work by including the necessary electronics, algorithms and communication modules in order to obtain a functional prototype. The final step in the project is to test a working prototype with a user.

2 State of the Art Load Monitoring Systems

The analysis of the human gait has proven to be beneficial, since changes in gait can reveal important information about people's quality of life. When studying human gait, two different approaches have been classified, i.e. gait systems based on 1) non-wearable sensors (NWS) and 2) wearable sensors (WS). NWS systems require a research facility with pre-installed sensors which capture the gait of the subject while walking on a marked walkway. WS systems, however, have the ability to gather information about the subject's gait outside the laboratory thus capturing his/her everyday activities. [15]

2.1 Gait Laboratories

NWS systems have usually been classified into two categories, i.e. systems utilizing image processing (IP), and those utilizing floor sensors (FS). The IP systems work by capturing the subject's gait using optic sensors thus acquiring kinematic data, but the FS system is based on sensors (pressure and ground reaction force sensors) which are located along the walkway the subject walks on during the experiment. [15]

By utilizing the force plate data and the tridimensional kinematic data obtained in conventional gait laboratories, estimation of joint forces and moments using inverse dynamic equations are made. This method involves a recursive process to compute forces and/or moments at each successive body segment of the subject, based on the subject's motion, starting with the segment in contact with the ground. [16] However, the forces and moments obtained using this method are somewhat limiting because of accumulation of error at each joint. This is due to the fact that forces and moments which are calculated at one given joint are used as input to obtain the forces and moments in the following joint. As an example, if the load on the abutment of a transfemoral amputee was to be estimated, the error calculated at the point of contact, the ankle joint, and the knee joint, would contribute to a large error seen at the abutment. Therefore, gait laboratories cannot reflect with 100% certainty what is truly happening at the abutment, although it gives a rough idea. Another limitation using gait laboratories is the limited amount of steps captured and the possibility of the gait being unnatural due to the subjects' tendency to "target" the force-plates [17]. The final limitation is how time consuming such studies can be, in addition to high costs, both due to facility renovations and equipment purchases that can be as high as \$300,000 [18].

2.2 Portable Monitoring Systems

It has long been known by researchers and clinicians that constant monitoring of forces and moments due to daily use of osseointegrated implant systems is important. Like noted before, having this information can be beneficial in designing an improved osseointegrated implant system in order to prevent mechanical failures, and to refine the rehabilitation protocol for amputees fitted with an osseointegrated prosthesis. [19]

Since conventional gait laboratories are limited when it comes to constant load monitoring, WS systems could be a better alternative. Many attempts have been made by researchers to create the optimal system. In 2008, Bamber *et al.* [20] e.g. developed a wireless gait analysis system called the "GaitShoe". This system allows

for constant data collection throughout the day in various environments which has not been possible with traditional motion laboratories. The system consists of a shoe with multiple sensor functions. For the kinematic motion analysis of the foot, two dual axis accelerometers and three gyroscopes are mounted on the backside of the shoe. In order to assess the pressure distribution of the foot and the timing parameters, strips of force sensitive resistors (FSRs) and polyvinylidene fluoride (PVDF) are placed inside the shoe, under the foot. Additionally, Bi-directional bend sensors are utilized to monitor flexion during gait, and electric field sensors to analyze the elevation of the foot. Although this system can offer constant monitoring, and does not interfere with the gait (which occasionally happens in laboratory environments), it still suffers from accumulation of errors when using inverse dynamic equations to calculate the forces and moments at proximal joints. This system would therefore not be optimal to use when trying to evaluate the forces and moments on the abutment of transfemoral amputees fitted with the OPRA Implant System.

Multiple studies have been conducted with the aim of understanding the different forces and moments that osseointegrated implant systems are exposed to [17][19][21][22][23][24][25][26]. Most of them use a portable transducer mounted between the abutment and the prosthetic leg to directly measure the load acting on the abutment, and consequently mitigating errors associated with the inverse dynamic method. In addition to minimizing errors, this approach gives a natural gait profile compared to experiments performed in gait laboratories.

In 2010, Frossard *et al.* [25][26] e.g. conducted two experiments where the aim was to measure directly the forces on the abutment during a fall, since falling is a great risk factor among lower limb amputees. In both studies, a six-channel transducer (Model 45E15A; JR3 Inc, Woodland, CA, USA) was used to record the loads on the abutment at frequency 200 Hz. These studies gave an insight for the first time into the kinetics of osseointegrated lower-limb prostheses and confirmed that a portable monitoring device can be very helpful in fall detection. The information gathered can also play a crucial role when it comes to designing automated wearable fall protective equipment, and like pointed out before, help with optimizing rehabilitation and exercise programs for patients fitted with osseointegrated implant systems.

Number of other experiments have been conducted where the commercially available six-channel transducer, JR3, mentioned above has been utilized. The setup of the transducer is however not always the same since the load cell is not designed solely for direct prosthetic gait monitoring, and has therefore been customized for each experiment. The communication platform differs also between experiments where some use tethered communications whereas others utilize wireless modems to transmit data.

An experiment executed by Lee *et al.* in 2007 [19] directly measured the load acting on the abutment of twelve active transfemoral amputees using the JR3 load cell mounted to customized plates which were positioned between the abutment (or the safety device if the amputee was fitted with such) and the prosthetic knee. A customized battery pack was used to power supply the transducer and kept in a waist pack secured on the subject. This system used a wireless transmitter in order to transmit the data from the transducer and to a near by computer. A picture of the setup can be seen in Figure 5. The results obtained in this study showed that there was a high subject-to-subject variability which indicates that the mechanical design of the

implants need to be either customized for each patient, or the design criteria for such implant systems need to be built around the highest force and moment values acting on the system within a wide range of amputees.

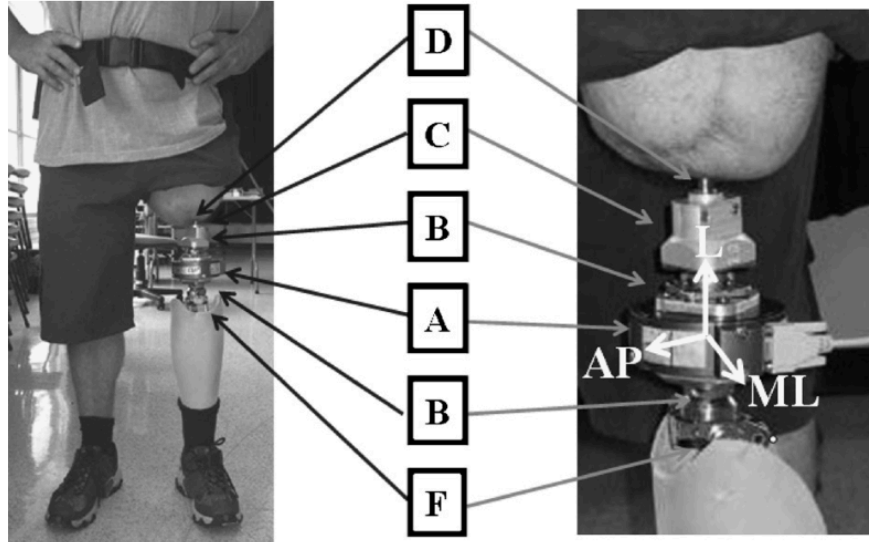


Figure 5: The setup of the prosthetic leg to directly measure the forces and moments acting on the abutment (left: front view, right: side view (L – long axis, AP – anteroposterior axis, ML – mediolateral axis)).

- A) Commercial transducer (JR3)
- B) Customized plates for the transducer
- C) Adaptor
- D) Abutment
- F) Prosthetic knee

Several other experiments have been conducted where the JR3 load cell is utilized: In 2008, Frossard *et al.* [23] performed an experiment to monitor the load regime acting on osseointegrated implant systems in transfemoral amputees to optimize the strength of the abutment in such systems. In 2010, Frossard *et al.* [22] conducted an experiment where load bearing rehabilitation exercises were monitored, highlighting the drawbacks of using weighing scales since off-axis loading cannot be monitored. In 2013, Frossard *et al.* [27] executed an experiment where the objective was to record inner-prosthesis loading of bone-anchored transfemoral prosthesis in order to confirm that changes of prosthetic components affect the inner-prosthetic loading, and thus providing key information for clinicians when it comes to selection of components for amputees.

In 2012, the prosthetic company College Park launched a 6-axis transducer called iPecs which is specifically designed to accurately measure 3-axis forces and moments in lower limb prosthetic users. The iPecs is capable of transmitting data wirelessly and into an on-board memory storage, which comes in handy since it allows for constant monitoring in real-world and clinical environments. [28][29] To the best knowledge of the author of this thesis, this is the only off-the-shelf load cells designed solely for load monitoring in lower-limb prosthesis.

In 2014, Koeler *et al.* [21] conducted an experiment to validate the accuracy of the iPecs system and did so by cross-validating its forces and moments with those obtained in a conventional gait laboratory. The results indicated that the forces and moments obtained with the iPecs were highly correlated with those measured by the gait laboratory ($r < 0.86$) which suggests that the iPecs is a viable alternative to conventional gait laboratories.

Although the iPecs systems is a stepping stone towards making constant load monitoring viable, it has its disadvantages. One is that it adds build height to the prosthesis which consequently can exclude users with long stumps (like all other commercial transducers used for this purpose like mentioned before). Another disadvantage is that if the iPecs should be used with the OPRA Implant system, it needs to be mounted between the Axor and the prosthetic knee, since the Axor has to be directly attached to the abutment. The read out values from the iPecs do therefore not represent exactly what happens at the abutment. The iPecs is also an expensive device, which limits its accessibility.

What all aforementioned experiments have in common is that they all contribute to a better understanding of the loading situation at the interface between the prosthesis and the human body, thus providing essential information which is important for engineers, researches and clinicians in understanding the kinetics of amputees fitted with osseointegrated implant systems. In addition, this information will help to improve the design of such systems (and other prosthetic components) and optimize the rehabilitation and exercise programs.

3 Theory

3.1 Strain Gauges

Strain gauges are used to measure strain in an object when a force or a moment is applied to it. They consist of an insulating flexible backing, which supports a metallic foil pattern positioned on top of it. Strain gauges are attached to the object of interest by using an adhesive, and once the object deforms, the strain gauges deform with it. As a result, the electrical resistance of the foil changes. This change is monitored using a Wheatstone bridge configuration, see Figure 6, and determines the strain according to the *gauge factor* (S_e) or the *sensitivity* of the strain gauge element, see (1), where dR is the change in resistance due to strain, R the resistance of the gauge before deformation, and e the strain. The gauge factor is known, and ranges from 2 to 6 for metallic foil gauges. [30]

$$\frac{dR}{R} = S_e e \quad (1)$$

A typical strain gauge is depicted in Figure 7 where the thin conductive strips are arranged in a zig-zag pattern. The strain gauges are much more sensitive in the direction of the parallel lines, i.e. a low stress value in that direction results in a large strain measurement and thus a large change in resistance. In order to monitor the change in the resistance, an excitation voltage must be applied to the input leads of the strain gauges (V_{Ex}). [30]

The supply voltage of the Wheatstone bridge is divided between the two halves of the bridge (R_1, R_2 and R_4, R_3), depending on the ratio of the corresponding bridge resistances, since each half of the bridge behaves as a voltage divider. The relationship between the output and input voltage can be seen in (2).

$$V_o = V_{Ex} \left(\frac{R_1}{R_1 + R_2} - \frac{R_4}{R_3 + R_4} \right) \quad (2)$$

When the bridge is balanced, i.e. when $R_1/R_2 = R_3/R_4$, the bridge output voltage (V_o) is zero. This should be the case when no force is applied to the object being measured. However, when the resistance in the strain gauge changes, the bridge becomes unbalanced, and the output voltage becomes nonzero. Since the change in output voltage is proportional to the change in resistance, the strain can be calculated as described in section 3.3. [31]

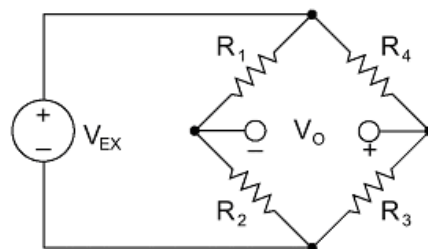


Figure 6: Wheatstone bridge [32].

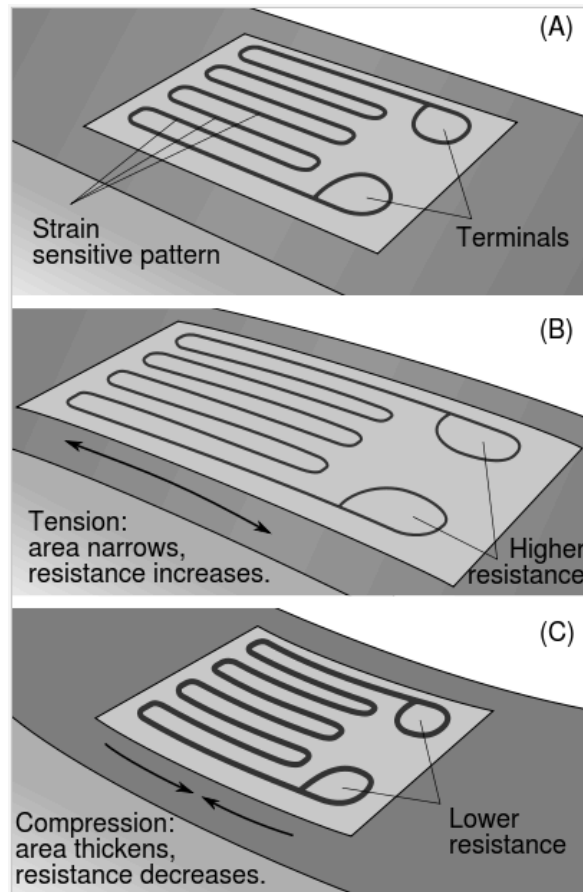


Figure 7: The working concept of a typical foil strain gauge attached to an object under exaggerated bending. A – no force applied, B – surface under tension (increased resistance), C – surface under compression (decreased resistance). [33]

3.2 The Measurement System

In practice, the strain measured by strain gauges is usually very small. This results in a very small change in resistance which is hard to measure directly using a conventional ohmmeter. Therefore, in order to determine the change in resistance, the strain gauge must be included in a measurement system. A typical diagram of such a measuring system can be seen in Figure 8. [31]

The measuring system is composed of several components. The first one is evidently the strain gauge itself, which converts, like noted before, mechanical strain into a change in electrical resistance. The second component is a completion circuit, which allows for the change in resistance to be measured. This measuring circuit is shown as a Wheatstone bridge in the diagram, where the strain gauge is used as one of the bridge arms. The measuring circuit together with the strain gauge are considered passive within the measuring system, i.e. energy must be supplied to them in order to acquire a meaningful signal. The power supply is usually a constant electrical voltage, but might as well be a constant current. [31]

Once the resistance of the strain gauge changes on account of the strain, the Wheatstone bridge becomes unbalanced since the bridge is no longer symmetric, and the change in output voltage observed is proportional to the change in resistance, as noted before. Since the change in output voltage is usually very small, a third component, an amplifier, must be included in the measuring system to obtain a relatively strong signal. Finally, the amplifier's output signal must be converted so that it can be easily observed. This is achieved by adding a fourth component to the measuring system, or a display (for example a voltmeter or ammeter). [31]

The components described above, only outline the essential items in the measurement system, but in practice, the system is often equipped with additional elements, such as filters, limit switches, peak value storages, etc. [31]

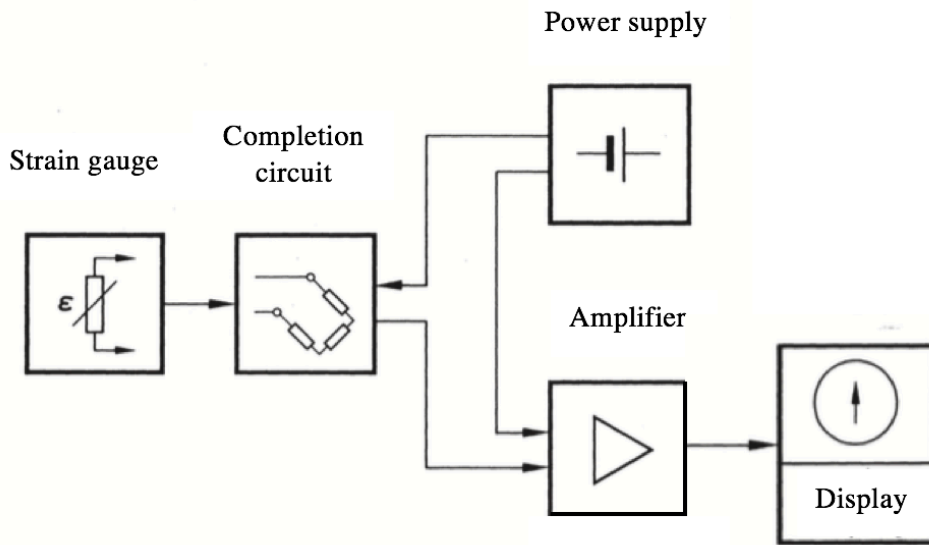


Figure 8: An illustration of a measurement system meant for measuring strain using strain gauges. (Figure adapted from [31]).

3.3 Wheatstone Bridge Configuration

In strain gauge technology, different forms of Wheatstone bridge circuits are used, and a few examples can be seen in Figure 9, where V_o represents the output voltage, V_{Ex} the input voltage, $R_{x(x=1,2,3,4)}$ (with arrows going through) the active strain gauges and $R_{x(x=1,2,3,4)}$ (with no arrows) the bridge completion resistors. The mounting and positioning of the strain gauges, determines what can be measured by the Wheatstone bridge. Although there are number of measuring modes for each Wheatstone bridge configuration, only one for each configuration will be described, three of which are used in this project (half, diagonal and full bridge). [31]

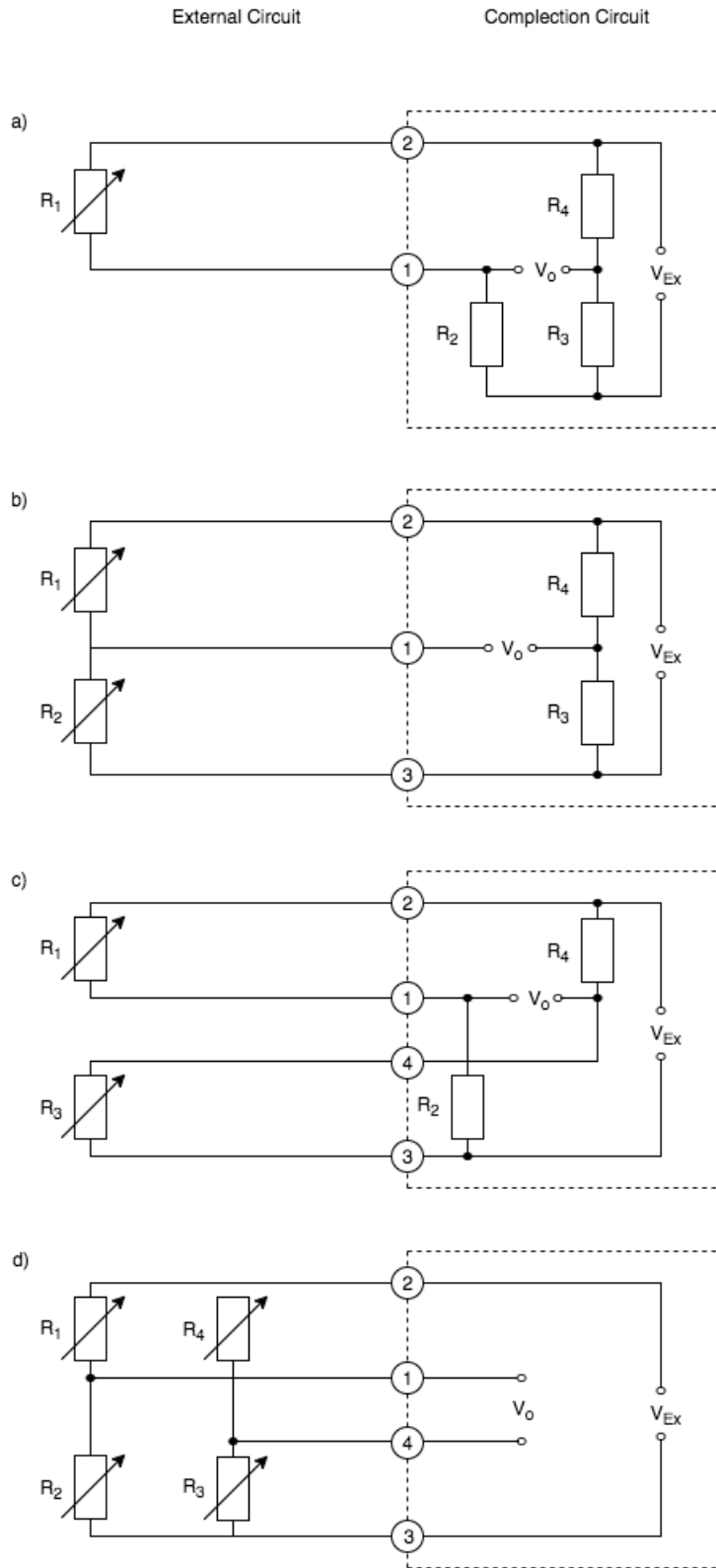


Figure 9: Wheatstone bridge configuration used in strain gauge techniques:

- a) quarter bridge
- b) half bridge
- c) double quarter or diagonal bridge
- d) full bridge

(Figure adapted from [31]).

Quarter bridge:

This configuration can measure either axial or bending strain. The bridge has only one active strain-gauge (R_1) which should be mounted in the direction of the axial or bending strain, see Figure 10. In order to convert the voltage measured to units of strain, the relationship in (3) can be used, where e represents the strain, ΔV_o the change in output voltage due to strain, V_{Ex} the excitation voltage, and S_e the gauge factor. [34][35]

$$e = \frac{4 \cdot \Delta V_o}{V_{Ex} \cdot S_e} \quad (3)$$

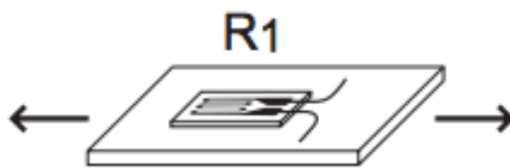


Figure 10: Example of a quarter bridge measuring mode [34].

Half Bridge:

This configuration can measure bending strain. The bridge has two active strain-gauge elements (R_1 and R_2), both of which are mounted in the direction of the bending strain but on opposite sides of the strain specimen, see Figure 11. This half-bridge configuration has the ability to compensate for temperature changes. The voltage to strain conversion can be conducted using the relationship seen in (4). [34][35]

$$e = \frac{2 \cdot \Delta V_o}{V_{Ex} \cdot S_e} \quad (4)$$

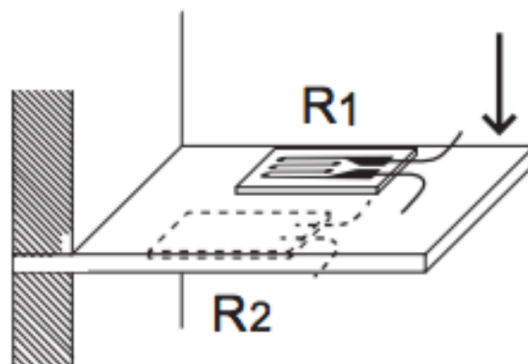


Figure 11: Example of a half bridge measuring mode [34].

Diagonal Bridge:

This configuration can measure axial strain. The bridge has two active strain-gauge elements (R_1 and R_3), which are both mounted in the direction of the axial strain but on opposite sides of the strain specimen, see Figure 12. The relationship seen in (5) shows how the voltage to strain conversion can be conducted. [34]

$$e = \frac{2 \cdot \Delta V_o}{V_{Ex} \cdot S_e} \quad (5)$$

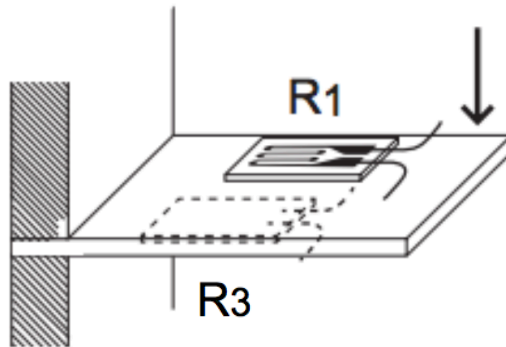


Figure 12: Example of a diagonal bridge measuring mode [34].

Full Bridge:

This configuration has the ability to measure torque. The bridge has four active strain-gauge elements (R_1, R_2, R_3 and R_4), two of them positioned on each side of the strain specimen at angles $\pm 45^\circ$ to the horizontal plane respectively, see Figure 13. The voltage to strain conversion can be conducted using the relationship seen in (6). [34]

$$e = \frac{\Delta V_o}{V_{Ex} \cdot S_e} \quad (6)$$

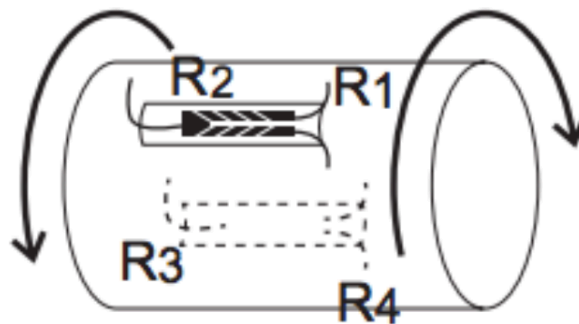


Figure 13: Example of a full bridge measuring mode [34].

3.4 Offset Nulling

Once the strain gauges have been mounted to the specimen, and the Wheatstone bridge has been completed, the output of the bridge is very seldom exactly zero, when no strain is applied to the specimen. That can be explained by a number of factors, e.g. variations in resistance of the Wheatstone arms, variations in lead resistance, and environmental factors such as temperature. This can be compensated for by performing offset nulling, either by software or hardware. [36]

- 1) **Software Compensation:** This method is convenient due to the fact that it is simple, fast, and does not need any manual adjustments. An initial measurement is taken before any strain is applied to the specimen. This measurement, which represents the offset of the bridge, is then used to correct subsequent measurements, by shifting them the same amount as the initial measurement. However, the downside is that the offset of the bridge is not removed which means that if the offset is very large, the gain of the amplifier applied to the output voltage will become limited due to saturation. Consequently, the dynamic range of the measurement will be limited. [36]
- 2) **Offset-Nulling Circuit:** The alternative method is a bit more complicated, since it requires manual adjustments, but has the advantage of completely removing the offset, and therefore does not restrict the dynamic range of the measurement. The method uses an adjustable resistance (potentiometer) which is incorporated into the hardware, and has the ability to be physically tuned. By adjusting the resistance of the potentiometer, the output of the Wheatstone bridge can be controlled, thus allowing for the initial output to be set to zero volts. [36]

3.5 Unit conversion

Axial, bending and torsional strain are common types of strain measured using strain gauge technology. To obtain meaningful data using strain gauges, it is important to convert the voltage read from the Wheatstone bridge to units of strain, see chapter 3.3. Once that has been achieved, the units representing axial force [N], bending moments [Nm] and torsional moments (torque) [Nm] can be found. To obtain the axial force and bending moments, Hooke's law is utilized, see (7), where σ represents the direct stress, e the strain and E the Young's modulus of elasticity. [31]

$$\sigma = e \cdot E \quad (7)$$

For the axial strain, the direct stress (σ_A) is found using the relationship in (8), where F_A stands for the axial load and A the cross sectional area. However, for the bending strain, the direct stress (σ_B) is found using the relationship in (9), where M_B represents the bending moment and S the sectional modulus. [31]

$$\sigma_A = \frac{F_A}{A} \quad (8)$$

$$\sigma_B = \frac{M_B}{S} \quad (9)$$

By inserting (7) into (8) and (9), the axial load (F_A) and bending moments (M_B) can be solved, see (10) and (11).

$$F_A = e \cdot E \cdot A \quad (10)$$

$$M_B = e \cdot E \cdot S \quad (11)$$

Now, by combining (4) and (11), and (5) and (10) respectively, the key equations for the conversion are obtained, see (12) and (13).

$$F_A = \frac{2 \cdot \Delta V_o}{V_{Ex} \cdot S_e} \cdot E \cdot A \quad (12)$$

$$M_B = \frac{2 \cdot \Delta V_o}{V_{Ex} \cdot S_e} \cdot E \cdot S \quad (13)$$

The torsional strain, however, is found with the relationship seen in (14) where τ represents the shear stress and G the shear modulus. The shear stress can then be calculated using the relationship seen in (15) where M_T represents the torsional moment (torque) and S_p the polar section modulus. [31]

$$e = \frac{\tau}{2 \cdot G} \quad (14)$$

$$\tau = \frac{M_T}{S_p} \quad (15)$$

By combining (14) and (15) the relationship for the torsional moment can be found, see (16).

$$M_T = 2 \cdot e \cdot S_p \cdot G \quad (16)$$

Finally, by inserting (6) into (16), the key equation for the conversion is obtained, see (17).

$$M_T = \frac{2 \cdot \Delta V_o}{V_{Ex} \cdot S_e} \cdot S_p \cdot G \quad (17)$$

4 Previous Work

As mentioned before, the groundwork for this project had already been conducted in a previous study [14]. It included the selection and location of strain gauges within the Axor and a prototyped acquisition system which was further improved in this work.

4.1 Selection of Strain Gauges

In the previous project, it was decided to monitor moments in all three axes, i.e. torsional moments and bending moments in both the anteroposterior (AP) and mediolateral (ML) direction, in addition to the force in the superior-inferior direction. The anatomical directional references are depicted in Figure 14 for explanation purposes.

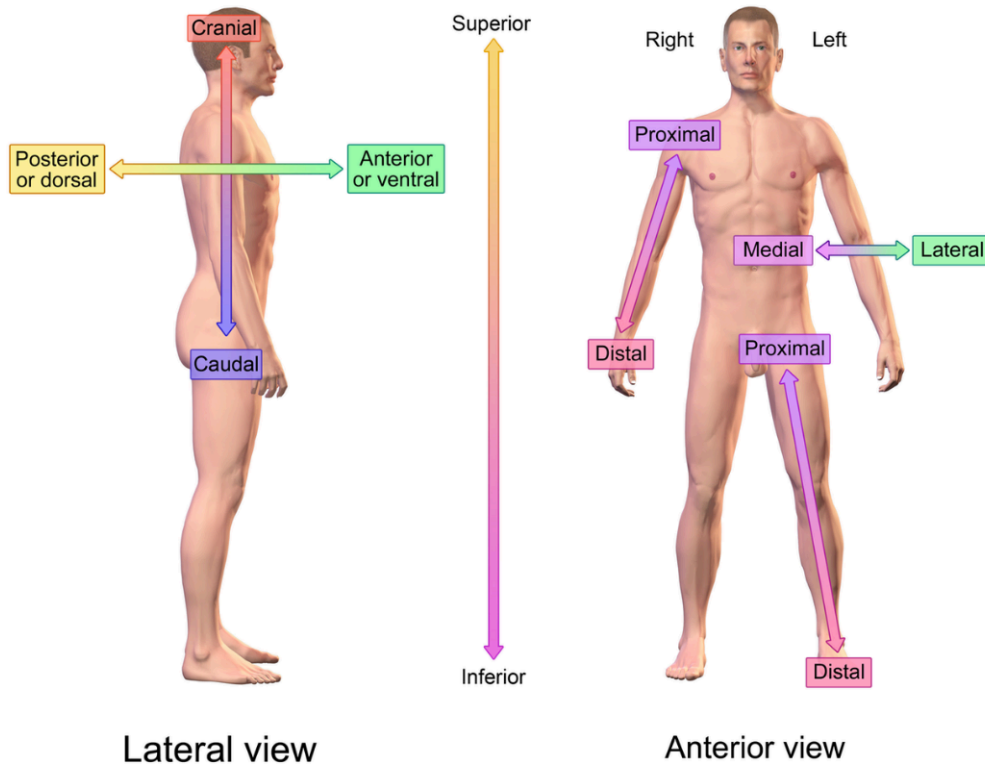


Figure 14: Anatomical directional references [37].

The reason why those forces and moments were chosen was due to the fact that they have proven to be the ones contributing to implant fractures in long term fatigue tests. The required Wheatstone bridge configurations for the chosen forces and moments can be seen in Figure 15, where the $R_{SGx(x=1,2,3,4)}$ represent the strain gauges mounted inside the Axor. As can be seen from the figure, a half bridge configuration is required for the bending moments, a diagonal bridge for the axial force, and a full bridge for the torsion. Therefore, 10 strain gauges were mounted inside the Axor, i.e. 4 strain gauges measuring bending moments in both the AP and ML direction, four strain gauges measuring torsion, and 2 strain gauges measuring axial force. The strain gauges chosen were from the Y-Series from HBM and all have the same resistance of **120 Ω** . [14]

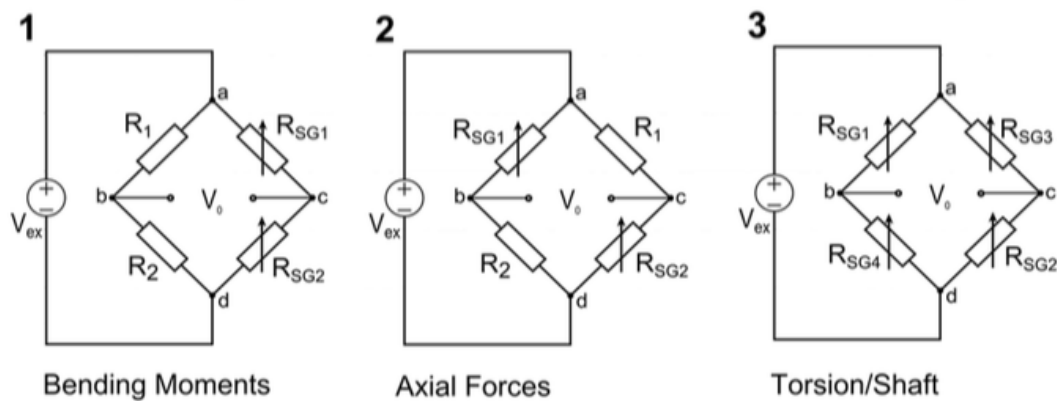


Figure 15: Wheatstone bridge configurations for chosen Axor measurements [14].

4.2 Placement of Strain Gauges and Signal Conditioning

The strain gauges were attached to a conical steel cylinder inside the Axor, which is in direct contact with the jaws clamping around the abutment, see Figure 16. Due to limited space, four different channels were milled into the aluminum part covering the conical cylinder, see Figure 17 – arrow 1, which allowed for all ten strain gauges to be mounted. Additionally, holes were drilled into the aluminum part, see Figure 17 – arrows 2 and 3, in order to lead the cables attached to the strain gauges out of the Axor. Four strain gauges were also attached to an abutment, in order to compare strain values and observe the load transfer from the Axor to the abutment. That way the Axor could be calibrated, so that the data coming from the Axor would represent forces and moments acting on the abutment. [14]

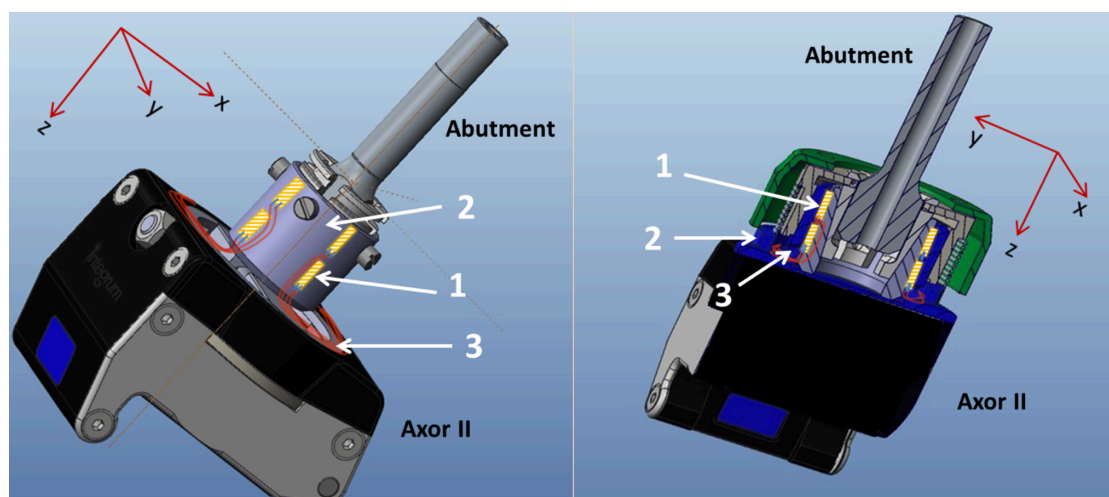


Figure 16: Placement of strain gauges (left), and the redesigned Axor fully assembled (right) [14].

- 1) Strain gauges
- 2) Conical steel cylinder
- 3) Cables

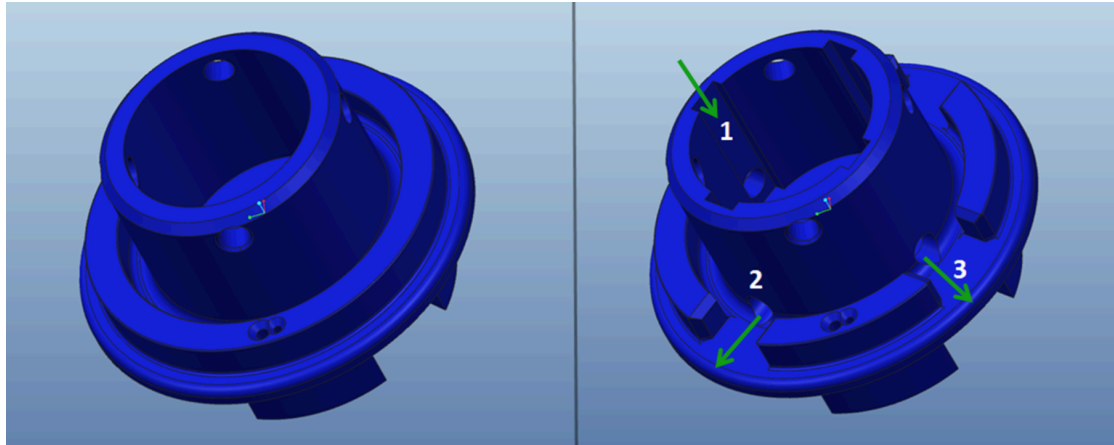


Figure 17: Unmodified Axor (left), and the redesigned Axor for instrumentation purposes (right). Arrow 1 demonstrates the milled channels, and arrows 2 and 3 the drilled holes. [14]

After the selection of strain gauges and their location inside the Axor, the necessary electronics were included which consisted of the following steps: 1) bridge completion, see Figure 15, 2) excitation, 3) amplification and 4) filtering. A detailed description of these steps is given in the thesis by Bregler (2016) [14]. A printed circuit board (PCB) was designed, which was compatible with the **Tiva™ C Series TM4C123G LaunchPad**, a microcontroller responsible for the analog to digital conversion (ADC) and other programmable features.

5 Methodology

5.1 System Requirements

After a background research had been conducted, the requirements the implemented device should satisfy were determined. Those requirements were as follows:

1) Signal Acquisition

- a. Hardware and software must be able to acquire signals (axial force, bending moments, torsion) from 5 different channels.
- b. Select an adequate sampling frequency so peak loads will not be disregarded.

2) Reliable data

- a. The data retrieved from the Axor must represent forces and moments acting on the abutment. Perform a calibration test (abutment vs. Axor) and a comparison test (Axor/abutment vs. iPecs).

3) Data storage

- a. The system must be able to store at least 7 days of continuous recording (excluding the night).

4) Communication – data transfer with a PC

- a. Data transfer between a Microcontroller Unit (MCU) and a computer must be reliable. The communication should be via SD (Secure Digital) card and the MCU should use the Universal Asynchronous Receiver-Transmitter (UART) port to output the data.

5.2 Repairing of Current device

Like mentioned before, the selection and location of the strain gauges, in addition to the necessary electronics to obtain a signal, had been achieved in previous work. Unfortunately, the designed PCB was not functioning at the start of this project, nor the majority of strain gauges attached to the Axor and abutment.

5.2.1 PCB

Due to dysfunction of the PCB, the first step was to order a new PCB to solder, see Figure 18, which has 5 channels, i.e. 3 measuring bending (channels 1, 2 and 3), 1 measuring axial force (channel 4), and 1 measuring torsion (channel 5).

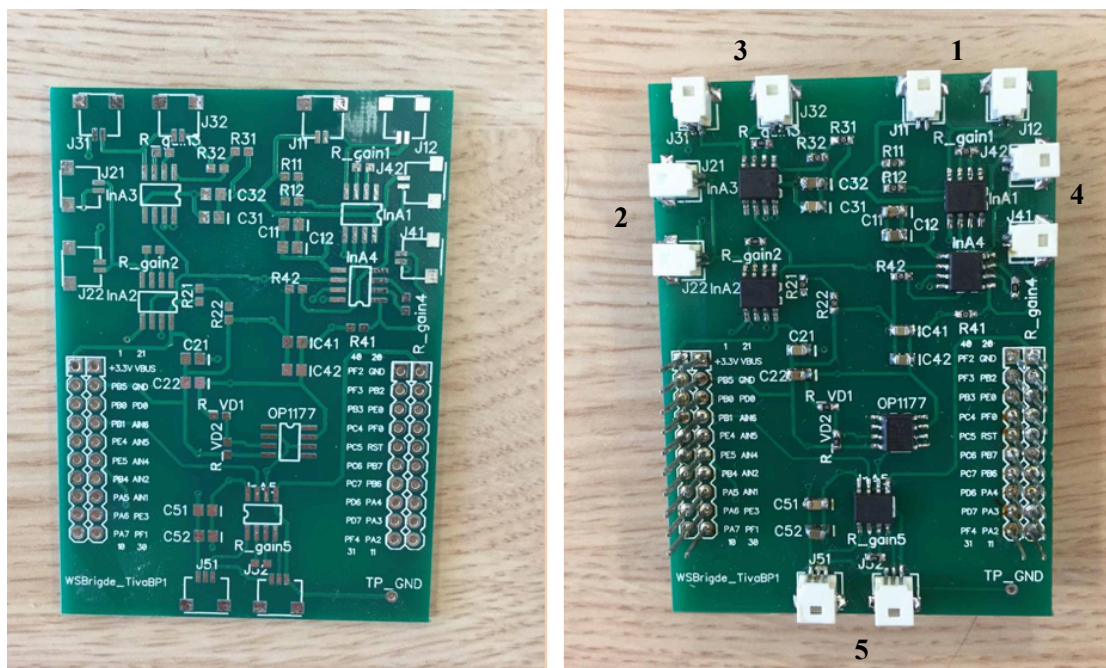


Figure 18: PCB before (left) and after (right) soldering.

5.2.2 Strain Gauges

The next step was to mount new functional strain gauges to the Axor and abutment. Before they could be mounted, the surface needed to be prepared to ensure good contact. The surface was scraped to remove any unwanted materials, and then smoothed out to eliminate debris that may have been created during the scraping. A cleaning solvent was applied to the surface to prepare it for bonding. After the thorough cleaning process, the surface was roughened by using an abrasive paper to improve the bonding even further. The surface was then cleaned again to free it of any unwanted debris that may have been created during the roughening process. Once cleaned, the strain gauges were mounted onto the surface. This was done by marking the area and then placing the strain gauge on the marked place on the object by using tweezers. An adhesive tape was used to keep the strain gauges in place while preparing the adhesive glue. Once the adhesive glue was ready to use, the tweezers were used to lift the strain gauges and then a thin layer of adhesive glue was applied on the mark. The gauges were then set down onto the adhesive and a steady even pressure was applied to them. After the adhesive had cured, the adhesive tape was removed with the tweezers, and an even pressure continued to be applied to the gauges for some time. [38]

The cables were soldered to the strain gauge terminals, and silicone glue applied on top of the whole installation, to prevent it from breaking. Figure 19 depicts the strain gauge installation for the abutment.

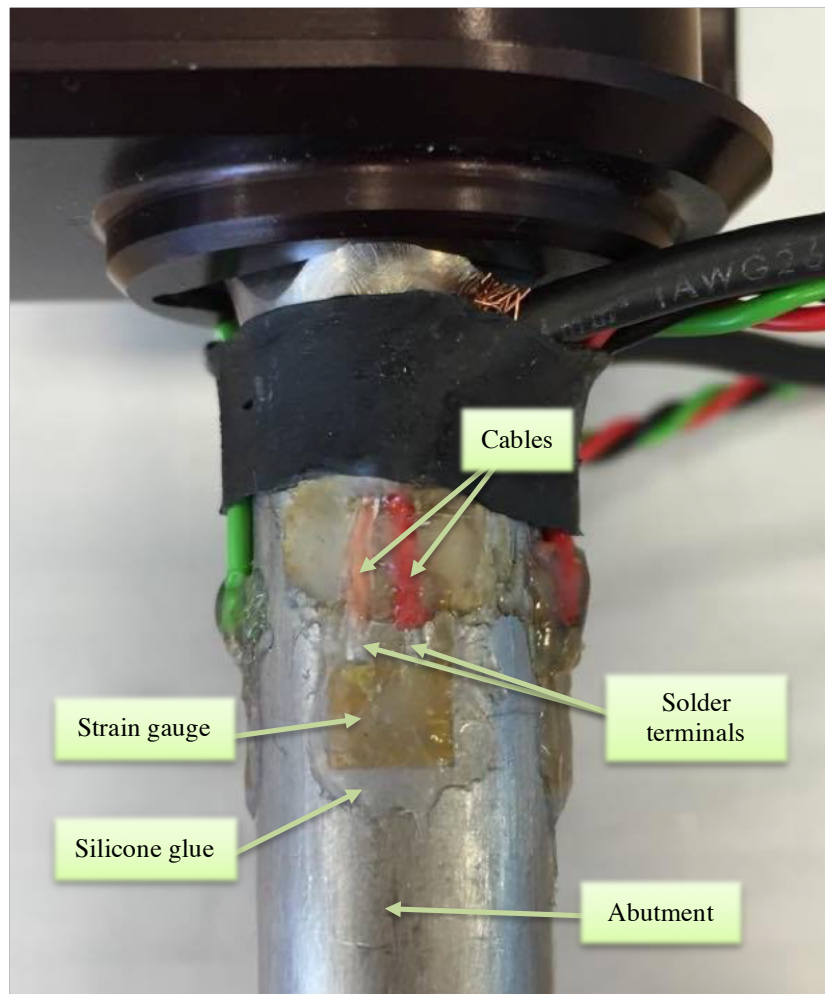


Figure 19: Strain gauge installation.

In total, six strain gauges were attached to the abutment, and ten to the Axor. Two strain gauges on the abutment measured axial force and bending (depending on the circuit configuration), and four measured torsion. In the Axor, two strain gauges measured axial force, four bending moments and four torsion.

5.3 Firmware

5.3.1 ADC Acquisition

A microcontroller compatible with the designed PCB was programmed, so that the analog signals obtained with the strain gauges could be converted into digital signals, thus allowing for the data to be stored and manipulated in a computer. The microcontroller used for this project, was an off-the-shelf product from Texas Instruments; **Tiva C Series TM4C123G Launchpad**, see Figure 20. The MCU was programmed using the integrated development environment (IDE) **Code Composer Studio** which is based on the **C/C++ Programming Language**. At the start of this project, a small program had been implemented, which was used as a starting point for this project and improved further. The basic requirements the MCU needed to fulfill in order to obtain and send data to a computer were as follows:

- 1) Enable the relevant General Purpose Input/Output (GPIO) pins on the Tiva and start the ADC conversion.
- 2) Send data from the MCU to the computer using an UART.

The ADC converter on the Tiva features a 12-bit conversion resolution, so in order to convert the binary data to voltage values, they needed to be multiplied with the voltage range of the Tiva and then divided by the number of codes which are dependent on the resolution of the board. For the Tiva, the voltage range is 0 – 3.3 V, and the number of codes are $2^{\text{resolution}} = 2^{12} = 4096$. Therefore, the theoretical resolution for the instrumented device was $3.3/4096 = 8.05 \cdot 10^{-4} \text{ V}$. [39]

Two programs were implemented, one for **real time communication**, and one for **SD card communication**. For the real time communication, the MCU needed to be connected to a computer, and the data sent directly to the UART. However, for the SD card communication, an SD card boosterpack had to be added, see Figure 21, which allowed for the data to be saved to an SD card.

For the real time communication, the microcontroller was programmed such that specific channels could be requested, i.e. only data from the requested channels would be sent to the computer, thus making the transmission process more efficient. For the SD card communication, the microcontroller was programmed in such a way that data coming from the strain gauges were saved to block indexes 2 and onward. The first block, however, stored a single number demonstrating how many blocks had been filled with memory. Knowing how many blocks had been filled ensured that data would not get overwritten should the device at some point be turned off and on again.

The sampling frequency of the MCU was determined with the aim of ensuring that important information would not be missed. However, the requirement that the instrumented device should store at least 7 days of continuous recording (see section 5.1), created a limitation since a very high sampling frequency would fill up the memory card quickly. A 16 GB SD card can e.g. store 4.000.000.000 samples (each of the size 4 bytes), which means that a sampling frequency higher than 1.000 Hz (given that data from 4 channels are being recorded), can not be chosen in order to fulfill the criteria. Therefore, the sampling frequency on the Tiva was chosen to be 1.000 Hz. That means that forces and moments with shorter duration than 1 msec can not be detected. This limitation should not effect the results too much, since forces and moments during daily activities are usually much longer in duration.

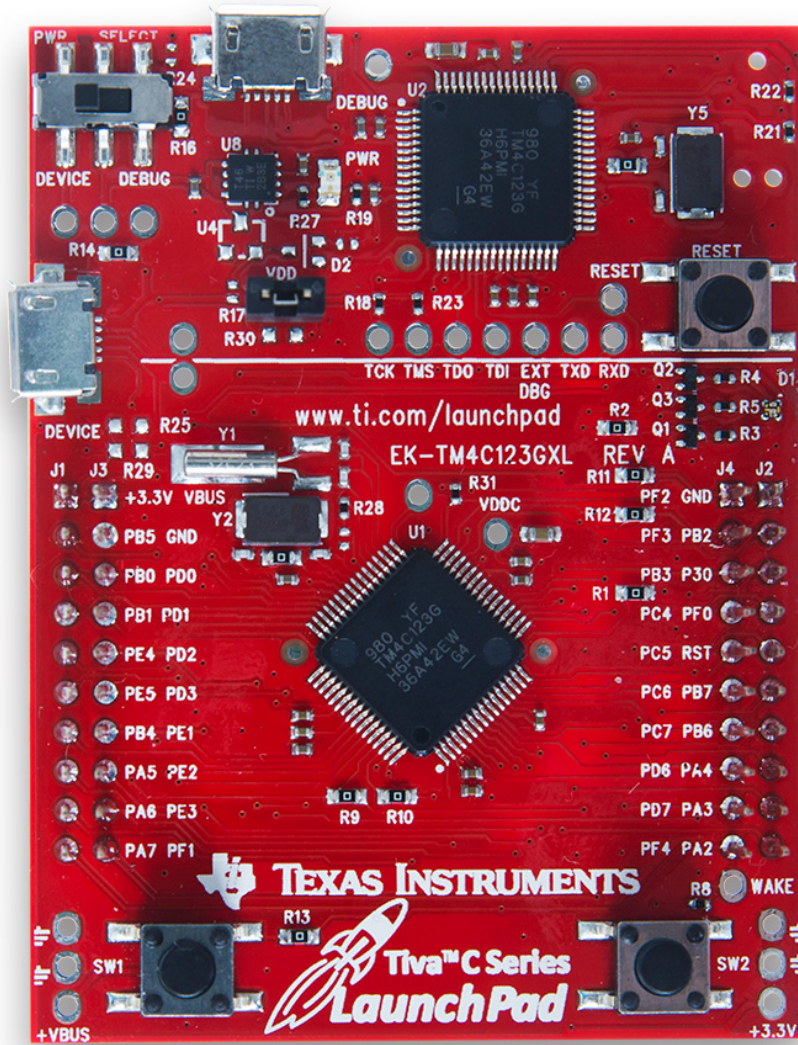


Figure 20: Tiva C Series Launchpad by Texas Instruments [40].

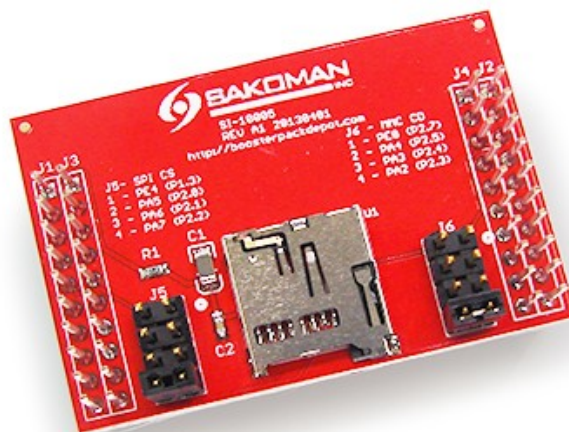


Figure 21: Micro SD Boosterpack [41].

5.3.2 PC Interface

In order to read data from the Tiva Launchpad, a user-friendly PC Interface was designed. This was achieved by creating a graphical user interface (GUI) in Matlab, see Figure 22, which has the ability to read data in real time and from an SD card. The features of the GUI are as follows:

- 1) Connect to the COM port for a USB communication.
- 2) For the real time communication, the following options can be chosen:
 - a. Test number.
 - b. Sampling time.
 - c. Time window for the plots.
 - d. Plot the data in real time, or plot the data once the sampling time has expired.
 - e. Enable specific channels on the PCB, and only retrieve data from them.
 - f. Start the data acquisition.
 - g. Stop the data acquisition.
- 3) For the SD card communication, the following options can be chosen:
 - a. Check the disk status.
 - b. See the memory usage of the SD card (by reading the block index saved in the first block).
 - c. Specify the block number and the starting address of the SD card.
 - d. Read the SD memory blocks, and save them to a file.

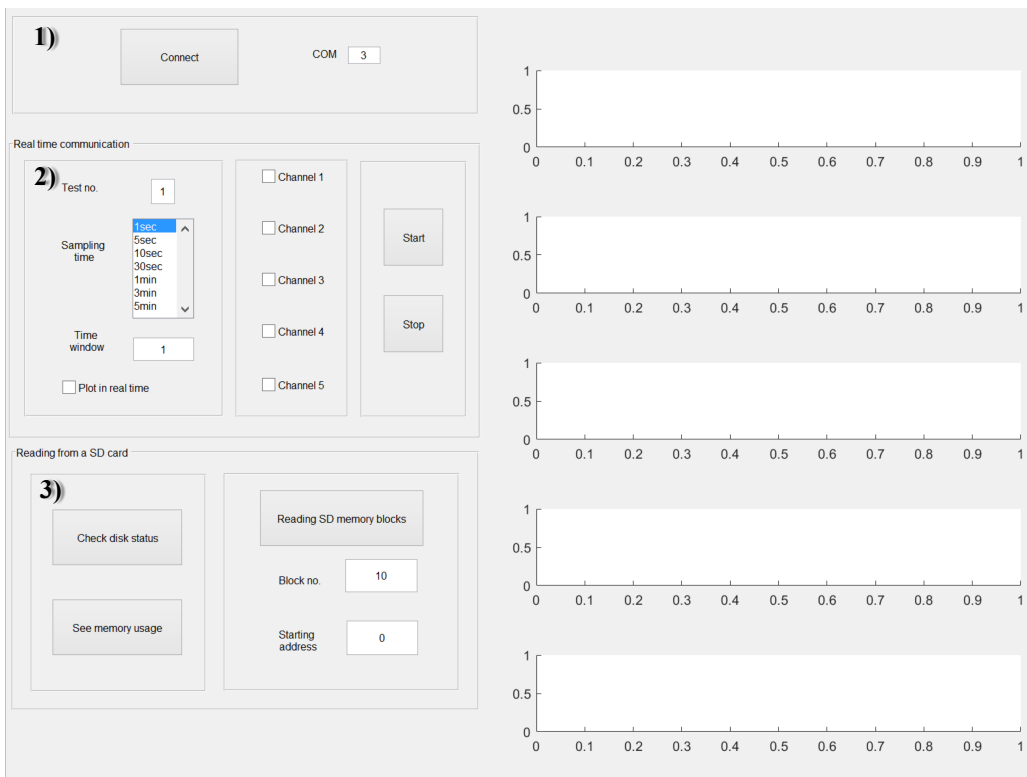


Figure 22: The custom designed GUI used to retrieve data from the MCU.

- 1) Connecting to the COM port to allow for a USB communication
- 2) Reading data in real time
- 3) Reading data from an SD card

5.4 Unit Conversion

The unit conversion was conducted by using the relationships seen in (12), (13) and (17).

Like (12) demonstrates, the cross sectional area (A) where the strain gauges are attached to the specimen, must be specified in order to obtain the axial force. The cross section area for both the abutment and the conical cylinder inside the Axor can be seen in Figure 23, and can be calculated using the relationship seen in (18), where D represents the outer diameter, and d the inner diameter [42].

$$A = \frac{\pi \cdot (D^2 - d^2)}{4} \quad (18)$$

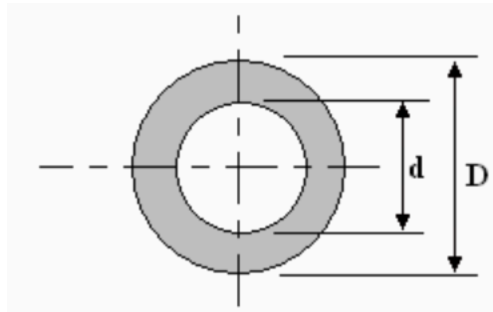


Figure 23: Illustration of a circular hollow section [43].

This gives the final relationship used to conduct the unit conversion for the axial load, see (19).

$$F_A = \frac{2 \cdot \Delta V_o \cdot E \cdot \pi \cdot (D^2 - d^2)}{4 \cdot V_{Ex} \cdot S_e} \quad (19)$$

In order to obtain the bending moment, the section modulus (S) must be specified, see (13). For a circular hollow section, the section modulus can be calculated using the relationship seen in (20) [42].

$$S = \frac{\pi \cdot (D^4 - d^4)}{32 \cdot D} \quad (20)$$

This gives the final relationship used to conduct the unit conversion for the bending moment, see (21).

$$M_B = \frac{\Delta V_o \cdot E \cdot \pi \cdot (D^4 - d^4)}{16 \cdot V_{Ex} \cdot S_e \cdot D} \quad (21)$$

For the torsional moment, the polar section modulus (S_p) must be specified, see (17). For a circular hollow section this can be calculated using the relationship seen in (22) [42].

$$S_p = \frac{\pi \cdot (D^4 - d^4)}{16 \cdot D} \quad (22)$$

This gives the final relationship used to conduct the unit conversion for the torsional moment, see (23).

$$M_T = \frac{\Delta V_o \cdot \pi \cdot (D^4 - d^4) \cdot G}{8 \cdot V_{Ex} \cdot S_e \cdot D} \quad (23)$$

5.5 Offset Nulling

The offset nulling was conducted by software since the PCB had already been designed at the start of this project. This was problematic at times since the offset of the bridge was not removed, and thus limited the gain of the instrumentation amplifiers on the PCB on account of saturation.

5.6 Instrumentation Amplifiers - Determining the Gain

In order to determine the gain of the amplifiers on the PCB, the maximum forces and moments the instrumented system should capture, needed to be decided upon. High moments should not be transferred to the implant due to the bend and rotation release in the Axor, which are set to certain threshold levels. However, should the Axor fail to release when the moments exceed the threshold limit, capturing those moments would be beneficial. Therefore, it was decided that the maximum moments the instrumented device should capture (without saturating) should be higher than the release level of the Axor. The chosen moments were **100 Nm** and **20 Nm** for bending and torsion respectively.

Since the Axor does not have a release mechanism depending on the axial force, the maximum axial force captured by the system needed to be determined in a different way. Since falling can be catastrophic for lower limb amputees fitted with osseointegrated implants (due to potential damage to the implant system), it seemed reasonable to base the chosen maximum force on the force transferred to an osseointegrated implant during a fall. In 2010, Frossard *et al.* [25] conducted a study where loads during a fall of a transfemoral amputee weighing 92.59 kg were monitored. According to the study, the maximum axial force applied to the implant during a fall was 1144.56 N. Therefore, the maximum force the instrumented device should capture was chosen to be **1200 N**.

Note that by increasing the range of the instrumented device, in terms of loads, the gain of the instrumentation amplifiers needs to be lowered to prevent them from saturating. This means that by increasing the range profusely, will result in a very vague signal. Therefore, the maximum forces and moments the device should capture were not chosen to be higher, to prevent the signal from being compromised.

After the maximum forces and moments had been determined, the gain of the instrumentation amplifiers was selected with the aim of fulfilling the criteria. In this project, the instrumentation amplifiers used were of the type 584-AD8226ARZ and are based on a 3-op-amp topology, see Figure 24. The gain of the amplifiers can be determined by placing a resistor across the R_G terminal seen in the figure, and can be calculated using the relationship in (24). [44]

$$Gain = 1 + \frac{49.4 \text{ k}\Omega}{R_G} \quad (24)$$

In order to determine the gain resistance (R_G) a simple test was conducted which will be described in the next section.

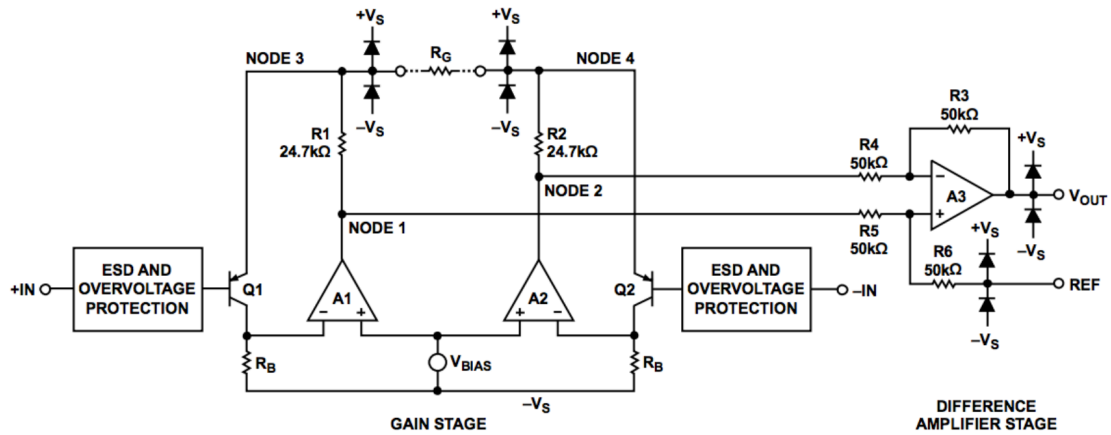


Figure 24: Schematic of the AD8226 [44].

5.7 Testing

5.7.1 Selecting Appropriate Gain Resistances

Test Purpose:

The test was meant to determine which gain resistances needed to be selected to ensure that the maximum forces and moments defined in section 5.6 could be captured by the instrumented device. The forces and moments of interest were as follows:

- Bending moment: **100 Nm**.
- Torsional moment: **20 Nm**.
- Axial force: **1200 N**.

Test Method:

Bending moments: The test was performed using a machine designed to apply bending forces, see Figure 25. The machine consists of a steel frame, two pneumatic actuators, and two load cells. The load cells are connected to each actuator which allows for applied loads to be monitored. The loads from the actuators are transferred to a tee piece, which is connected to a fixture. The instrumented abutment was screwed into the fixture, and the instrumented Axor mounted to the bottom part of the machine. Finally, the abutment was fitted into the Axor and fastened securely. The cables coming from the strain gauges measuring bending (in both the abutment and Axor) were plugged into the PCB (channels 1, 2 and 3), which was mounted on top of the Tiva. The Tiva was connected to a computer and the Matlab GUI used to control the communication. The sampling frequency was set to 500 Hz. The load applied to the tee piece was 1000 N, which equals **100 Nm** since the distance from the center of the actuator and the fixture holding the abutment is 0.1 m. The frequency of the actuators was set to approximately 0.8 Hz and the recording session was 10 sec, which gave approximately 13 bending cycles. The test was performed a number of times, with different gain resistances, until the instrumentation amplifier was not saturated. Figure 26 depicts the test setup.

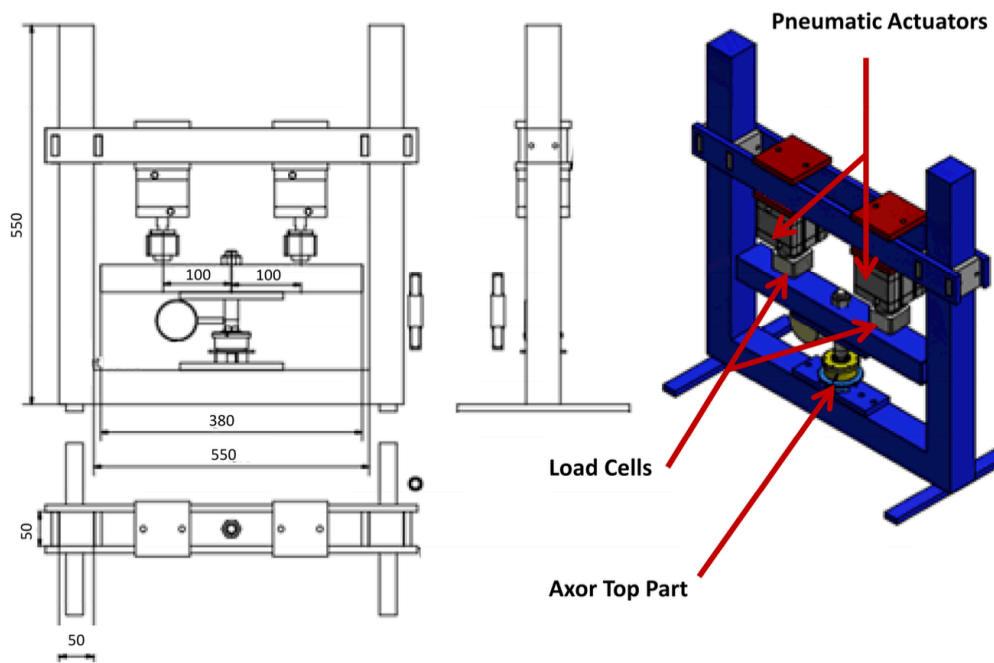


Figure 25: Test machine for measuring bending. (Image provided courtesy of Integrum AB).

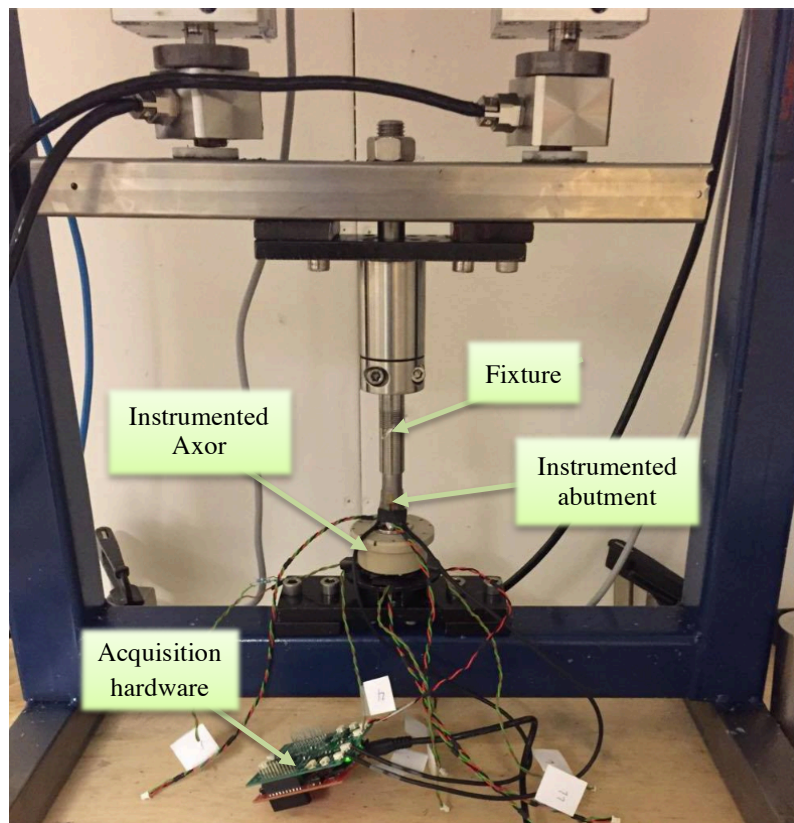


Figure 26: Test setup – Selecting gain resistances for bending moments.

Torsional moments: In this test, the instrumented abutment was securely fitted inside the instrumented Axor, and then the assembly mounted in a vise, see Figure 27. The cables coming from the strain gauges measuring torsion (in both the abutment and Axor) were plugged into the PCB (channel 5), which was mounted on top of the Tiva.² The Tiva was connected to a computer and the Matlab GUI used to control the communication. The sampling frequency was set to 500 Hz. A conventional torque wrench was used to apply approximately **20 Nm** to the abutment. The test was performed a number of times, with different gain resistances, until the instrumentation amplifier was not saturated.

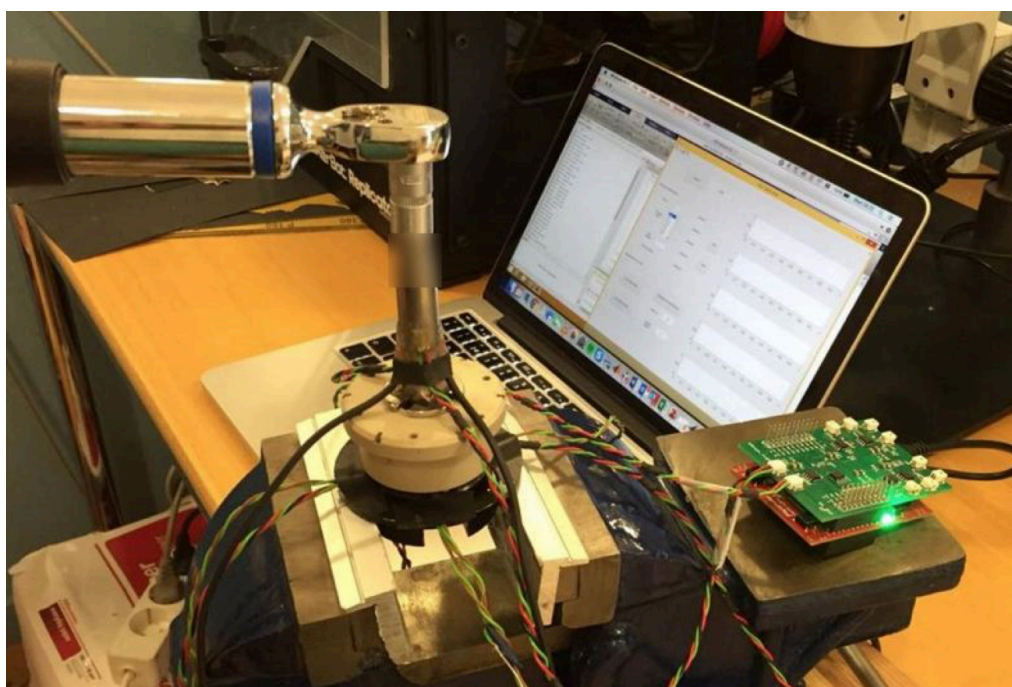


Figure 27: Test setup – Selecting gain resistance for torsional moments.

Axial force: A non-conventional test method was developed for measuring the axial force (since Integrum is not equipped with a test machine capable of measuring axial force)³. In this experiment, the instrumented abutment was fitted inside the instrumented Axor and fastened securely. Then the assembly was placed on the floor and the cables coming from the strain gauges measuring axial force (in both the abutment and Axor) were plugged into the PCB (channel 4) which was mounted on top of the Tiva.⁴ The Tiva was connected to a computer and the Matlab GUI used to control the communication. The sampling frequency was set to 500 Hz. A person weighing approximately 90 kg was finally asked to step onto the abutment and jump lightly. An assumption was made that the force applied would be close to **1200 N**. The test was performed a number of times, with different gain resistances, until the instrumentation amplifier was not saturated.

² Note that the PCB has only one channel measuring torsions. Therefore, the test for the abutment and Axor needed to be conducted separately.

³ Note that the test machine measuring bending could have been utilized with some modifications, but due to time restrictions different method was chosen.

⁴ Note that the PCB has only one channel measuring axial force. Therefore, the test for the abutment and Axor needed to be conducted separately.

5.7.2 Calibration Test

Test Purpose:

The aim of this test was to calibrate the data from the Axor such that they represent forces and moments acting on the abutment.

Test Method:

Bending moment: The same test setup as described in section 5.7.1 (Selecting Appropriate Gain Resistances – Bending moment) was used to conduct the bending calibration. A load of 1000 N, or **100 Nm**, was applied 4 times in a row on each side of the tee piece alternately. The sampling frequency was set to 1000 Hz and the recording session was 2 minutes. The experiment was performed two times where the Axor was rotated 90 degrees, since the Axor can measure bending in two directions (AP and ML).

Torsional moment: For the torsion calibration, the same test setup as described in 5.7.1 (Selecting Appropriate Gain Resistances – Torsional moment) was used. A load of **20 Nm** was applied to the abutment, 5 times in each direction alternately. The sampling frequency was 1000 Hz and the recording session 3 minutes. Due to the fact that the PCB has only one channel measuring torsion, the instrumented Axor and abutment could not measure at the same time. Therefore, the test had to be conducted separately, first for the Axor and then for the abutment, where the gain resistance was changed between runs.

Axial force: The results obtained in the test described in chapter 5.7.1 (Selecting Appropriate Gain Resistances – Axial force), indicated that no signal was detected from the axial strain gauges inside the Axor (see chapter 6.2.1). Therefore, the test was not performed for the axial force.

After having conducted the test, the obtained datasets (bending moment and torsional moment) were manipulated to perform the offset nulling and to mitigate noise. The offset nulling was performed by utilizing the Matlab function ‘detrend’, which removes the mean value from the data, and the noise mitigation was conducted by band pass filtering the data with the cutoff frequencies 0.0001 Hz and 10 Hz. Finally, the calibration was conducted by using the Curve Fitting Toolbox in Matlab, where a linear model describing the relationship between the Axor and abutment data was obtained.

5.7.3 Comparison Test

Test Purpose:

The objective of this test was to compare moments and forces measured by the iPecs, a commercially available 6-axis transducer, with the instrumented Axor and abutment.

Test Method:

Bending moment: The instrumented Axor was fully assembled and mounted on top of the iPecs. The instrumented abutment was then fitted into the Axor and fastened securely. Finally the whole assembly was fixed to the bottom part of the test machine described in chapter 5.7.1 (Selecting Appropriate Gain Resistances – Bending

moment), see Figure 28. Note that the build height of the assembly was too high for the test machine, so the only purpose of the machine was to fix it securely but not to apply any load to it. The cables coming from the strain gauges measuring bending (in both the abutment and Axor) were plugged into the PCB (channels 1, 2, and 3), which was mounted on top of the Tiva. The Tiva was connected to a computer where the sampling frequency was set to 1000 Hz, and the Matlab GUI used to control the communication. Another computer was used to connect to the iPecs wirelessly, where the sampling frequency was also set to 1000 Hz. Since the test machine could not be used to apply loads to the assembly (due to the increased build height), hand power was used instead where the proximal part of the abutment was pushed and pulled alternately (twice in each direction). The test was conducted three times, i.e. once when measuring from the instrumented abutment (and iPecs), and twice when measuring from the instrumented Axor (and iPecs), where the Axor was rotated 90° between tests (AP and ML direction). The recording time for each test was 1 minute.

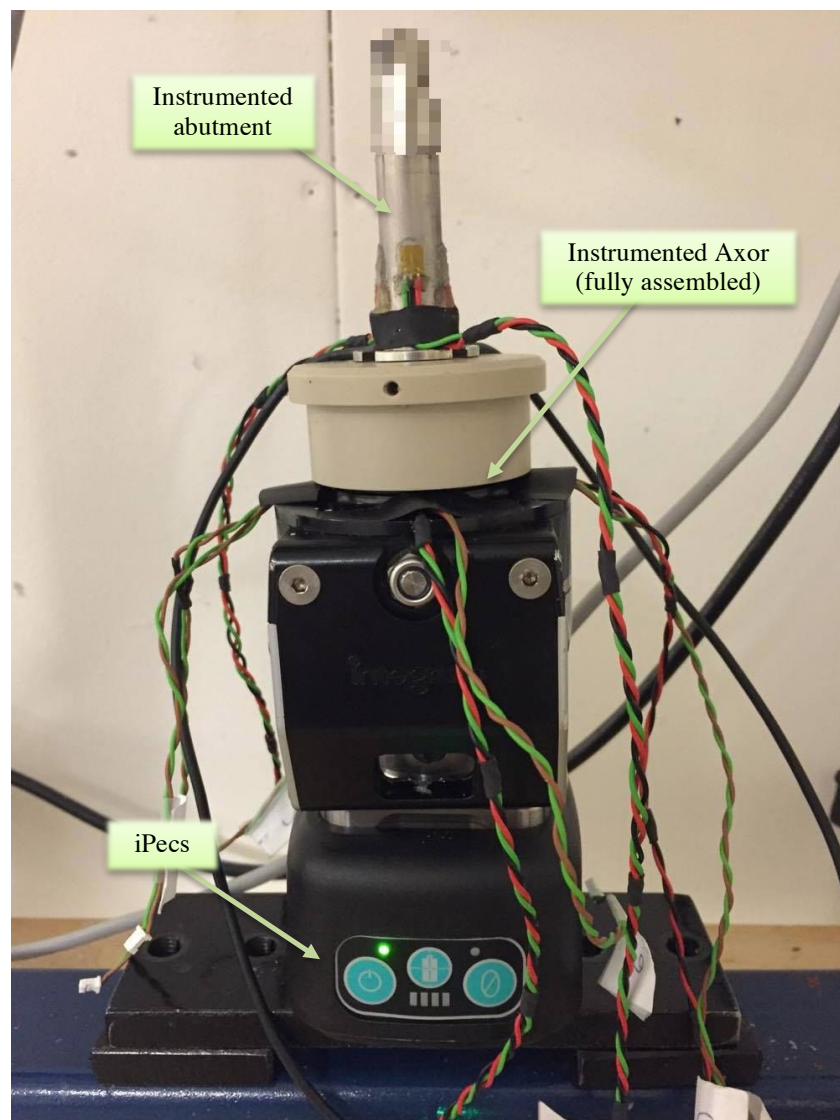


Figure 28: Test setup – Bending comparison.

Torsional moment: The setup for this test was the same as in the bending moment comparison, see Figure 28. The only difference was that the cables coming from the strain gauges measuring torsion (in both the abutment and Axor) were plugged into the PCB (channel 5), and a conventional torque wrench was used to apply approximately 10 Nm to the abutment in both directions. The test was conducted two times⁵, i.e. once when measuring from the instrumented abutment (and iPecs) and once for the instrumented Axor (and iPecs). The recording time was 3 minutes.

Axial force: For the axial force comparison, the whole assembly was placed on the floor and the cables coming from the strain gauges measuring axial force in the abutment plugged into the PCB (channel 4). A person weighing approximately 60 kg then stepped on and off the assembly while recording the axial force measured by both the instrumented abutment and the iPecs. The test was only conducted one time, since the instrumented Axor was not able to measure axial force (see chapter 6.2.1). The recording time was 25 seconds.

Once the test had been conducted, all datasets (bending moments, torsional moments, axial force) were filtered digitally, following the same filter procedure described in the calibration test, in order to mitigate noise and perform the offset nulling. Additionally, the unit conversion (see section 5.4) was conducted prior to the comparison since the iPecs is measuring in Newtons/Newton-meters.

5.7.4 SD Card Communication

Test Purpose:

The aim of this test was to verify that the SD card communication is reliable, by comparing the obtained results with real time communication data.

Test Method:

The instrumented abutment was fitted inside a fixture and the cables coming from the strain gauges measuring bending were plugged into channel 1 on the PCB. A boosterpack for an SD memory card was then mounted on top of the PCB, which in turn was mounted on to the Tiva, see Figure 29. The Tiva was connected to a computer and the Matlab GUI used to control the communication where the sampling frequency was set to 500 Hz. Figure 30 depicts the setup for the experiment. A force was then applied to the proximal part of the abutment using hand power and the change in voltage monitored for 50 seconds. The measured data was both saved to the SD card and sent directly to the computer through the UART. The two dataset were then compared with the aim of confirming that the SD card communication was reliable.

⁵ Note that the gain resistance needed to be changed on the PCB between tests.



Figure 29: The acquisition hardware – Tiva (bottom), PCB (middle), boosterpack for an SD memory card (top).

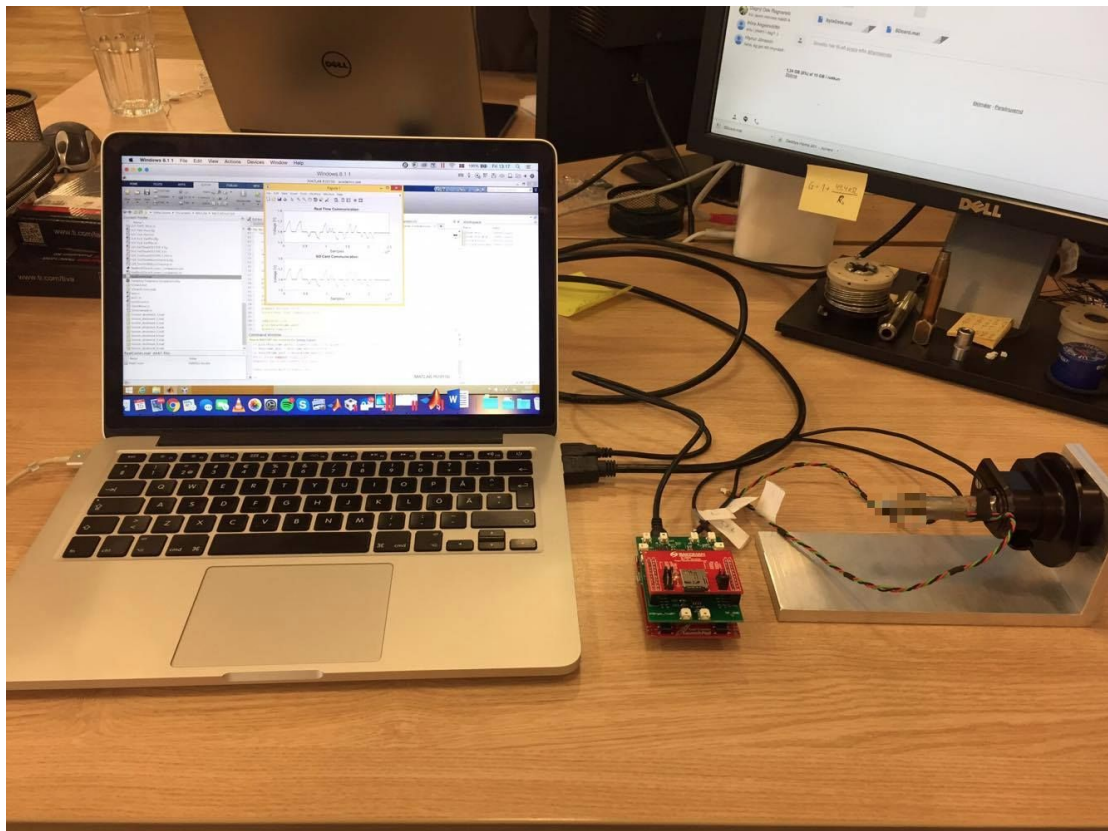


Figure 30: Test setup – SD card communication.

5.8 External Battery

Since the instrumented Axor should monitor forces and moments applied to the abutment throughout daily activities, a rechargeable 7.4 Volt Lithium-Ion battery was used to power the device. Additionally, an external voltage regulator was added to the system, see Figure 31, due to the fact that the Tiva can not handle voltages higher than 5.5 V [45]. The leads of the battery were soldered to the input of the regulator, and the cables from the output of the regulator soldered to the Tiva, see Figure 32.

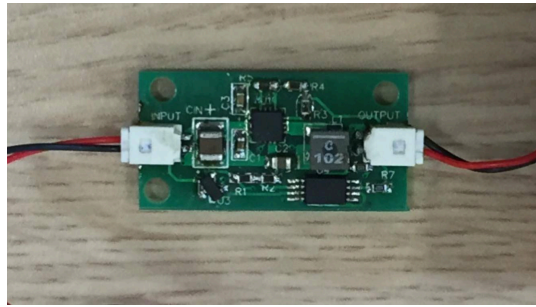


Figure 31: The voltage regulator.

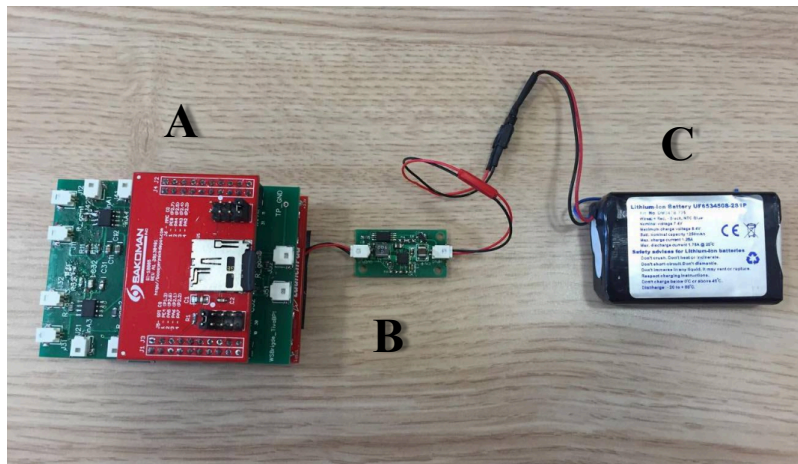


Figure 32: The acquisition hardware (A) connected to the voltage regulator (B) which in turn is connected to the external battery (C).

5.9 Housing for the Electronics

A housing for the electronics and the battery was designed to allow for patients to wear the device. The housing was modelled using the 3D program **PTC Creo**, and had three openings to access the channels measuring bending (AP and ML) and torsion. The channel for the axial force did not need to be accessed due to the fact that the instrumented Axor was not capable of measuring axial force (see chapter 6.2.1). Since the device should monitor forces and moment continuously, the battery needed to be recharged daily. Therefore, a charging port was added to the box, and consequently a switch, which allowed the patient to choose between a recording or a charging mode of the device. Finally, a Velcro was attached to the lid of the box to allow it to be fastened to the patient. The housing can be seen in Figure 33.

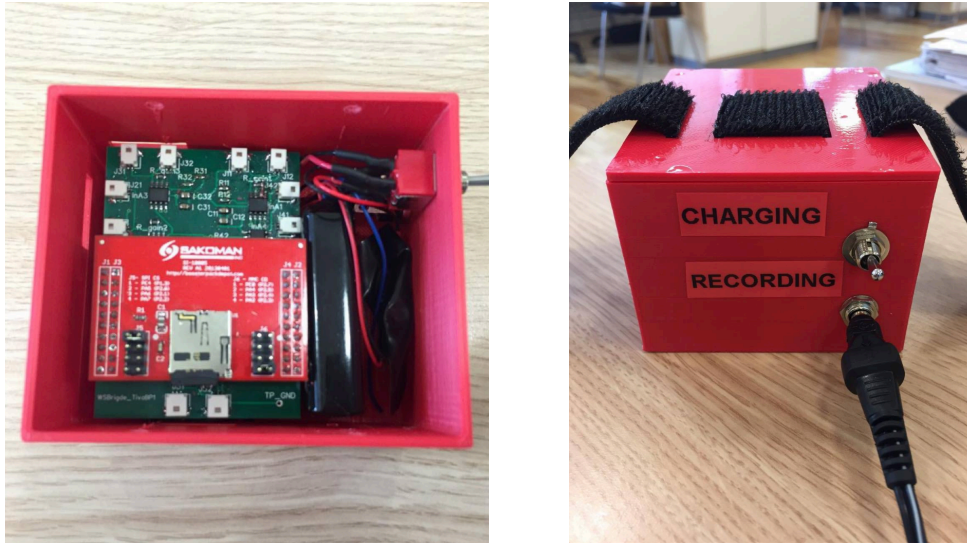


Figure 33: Housing for the electronics.

5.10 Patient Pilot

The implemented device was finally tested with a user for a short period of time.⁶ Since the axial force could not be measured with the instrumented Axor, the plan was to measure only bending moments and torsion. However, on the day of the test, the torsion channel on the PCB was not functioning for some reason, and therefore only bending moments were recorded. The test took place at Integrum's office where a patient was fitted with the instrumented Axor, and the housing containing the electronics attached to the patient with the Velcro (see Figure 34). The device was aligned such that two of the strain gauges measuring bending were coaxial with the AP axis (anterior set to positive), and the other two coaxial with the ML axis (lateral set to positive). The sampling frequency of the device was set to 1000 Hz, and the data was saved to an SD card. The patient participating in the experiment was a low active 76-year-old male, amputated since 1986, and had been fitted with the OPRA Implant System since 1999. Three recording sessions with the patient were conducted where he was asked to perform number of activities. In the first recording session the patient walked back and forth on a normal pace for a few minutes. In the second recording session the patient was asked to sit down and stand up number of times. In the third recording session the patient was asked to apply as much voluntary load to the abutment in the AP direction while sitting down. This was conducted by having another person holding the prosthesis fixed in a horizontal direction, while the patient tried to either lift or press down the foot.

Once the datasets had been collected, they were filtered digitally, following the same filter procedure as described in the calibration test, in order to mitigate noise and perform the offset nulling. In addition, the datasets were calibrated using the linear models obtained in the calibration test, to monitor forces and moments acting on the abutment.

⁶ Ethical approval from the Regional Ethics Committee in Gothenburg was granted for this experiment.



Figure 34: Patient fitted with the instrumented device.

6 Results

6.1 Unit Conversion

The unit conversions were easy to conduct once the equations were known (see chapter 5.4). The parameters seen in Table 1 were used for the conversion [46][47]. Note that the Young's modulus (E) and shear modulus (G) depend on the material which the strain gauges are attached to. For the abutment, the material is titanium alloy, but for the conical cylinder inside the Axor, the material is stainless steel.

Table 1: Parameter for the unit conversion.

Parameter	Symbol	Unit	Abutment	Axor
Gauge factor	S_e	-	1.93 ± 1.5% (axial force/bending) 1.90 ± 1.5% (torsion)	
Young's modulus of elasticity	E	GPa	105	193
Shear modulus	G	GPa	41.0	78.0

The calculated results for the unit conversion can be found in Table 2.

Table 2: Unit conversion – Test results.

Parameter	Unit	Abutment	Axor
Bending moment	Nm	$6.8 \cdot 10^3 \cdot \Delta V_o$	$1.1 \cdot 10^5 \cdot \Delta V_o$
Torsional moment	Nm	$5.3 \cdot 10^3 \cdot \Delta V_o$	$9.3 \cdot 10^4 \cdot \Delta V_o$
Axial force	N	$3.4 \cdot 10^6 \cdot \Delta V_o$	$1.8 \cdot 10^7 \cdot \Delta V_o$

6.2 Testing

6.2.1 Selecting Appropriate Gain Resistances

Since all channels suffered from an offset in the baseline, the gain was chosen to be a bit lower than the theoretical gain, to ensure that the instrumentation amplifiers would not get saturated in one direction.

The results for the selected gain resistances can be seen in Table 3.

Table 3: Selecting appropriate gain resistance – Test results.

Load	Parameter	Unit	Abutment	Axor
Bending moment (100 Nm)	Gain resistance	Ω	499	50
Torsional moment (20 Nm)	Gain resistance	Ω	153	35
Axial force (1200 N)	Gain resistance	Ω	40	-

As can be seen in Table 3 no resistance was chosen for the axial force in the Axor. This is due to the fact that no signal was obtained from those strain gauges, even though the resistance was very low, and the force applied to the device was very high.

6.2.2 Calibration Test

Bending moment:

The following graphs show the results obtained in the bending calibration. Figures 35 and 36 depict 13 seconds (16 bending cycles) of recorded data (after filtering) from both the Axor and abutment, where volts are plotted against time. Figures 37 and 38, in turn show the comparison between the calibrated Axor data and the abutment data.

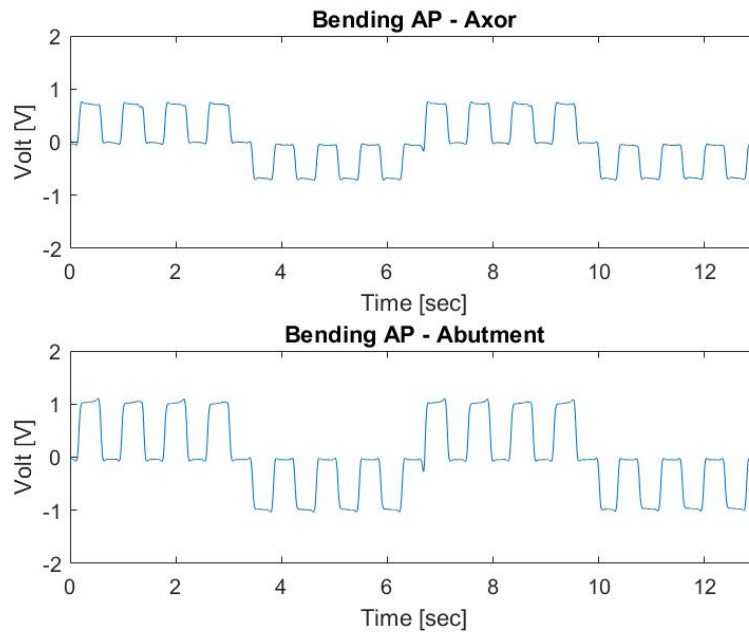


Figure 35: Bending moments around the AP axis measured by the Axor and abutment.

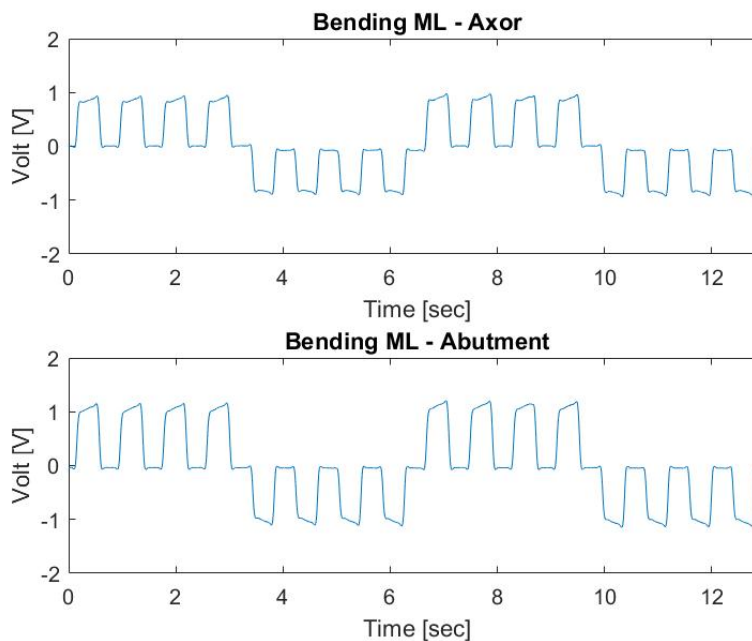


Figure 36: Bending moments around the ML axis measured by the Axor and abutment.

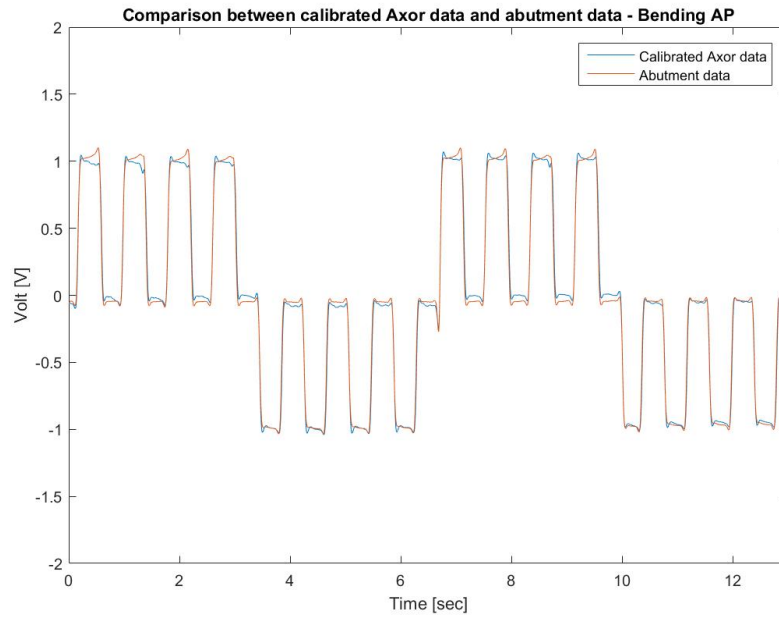


Figure 37: Comparison between the calibrated Axor data and the abutment data – Bending around the AP axis.

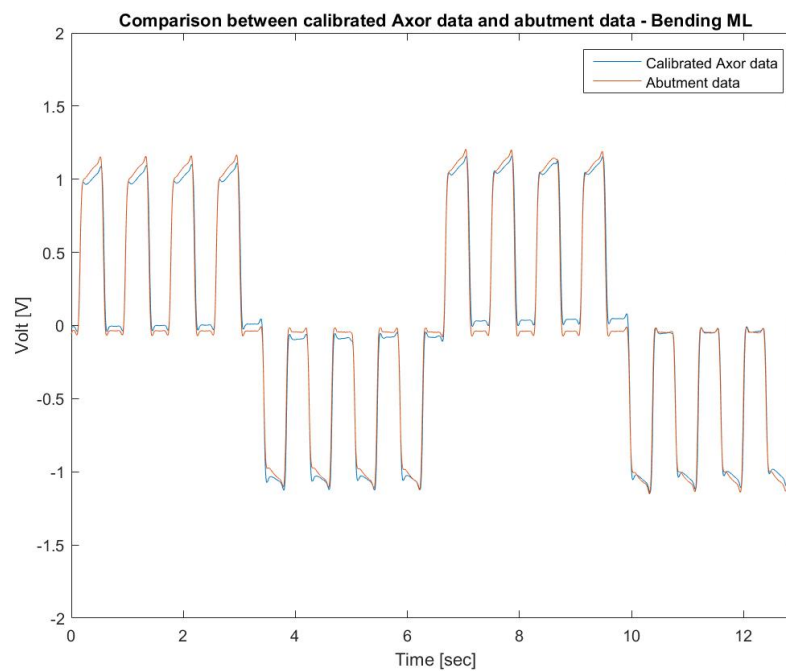


Figure 38: Comparison between the calibrated Axor data and the abutment data – Bending around the ML axis.

Torsional moment:

Figure 39 shows 29 loading cycles obtained from both the Axor and abutment (after filtering), where volts are plotted against time. As can be seen on the graphs, the linear relationship between the two signals is very poor, which made the calibration impossible. Hence, the calibration for the torsional moments was not conducted since the results would be unreliable.

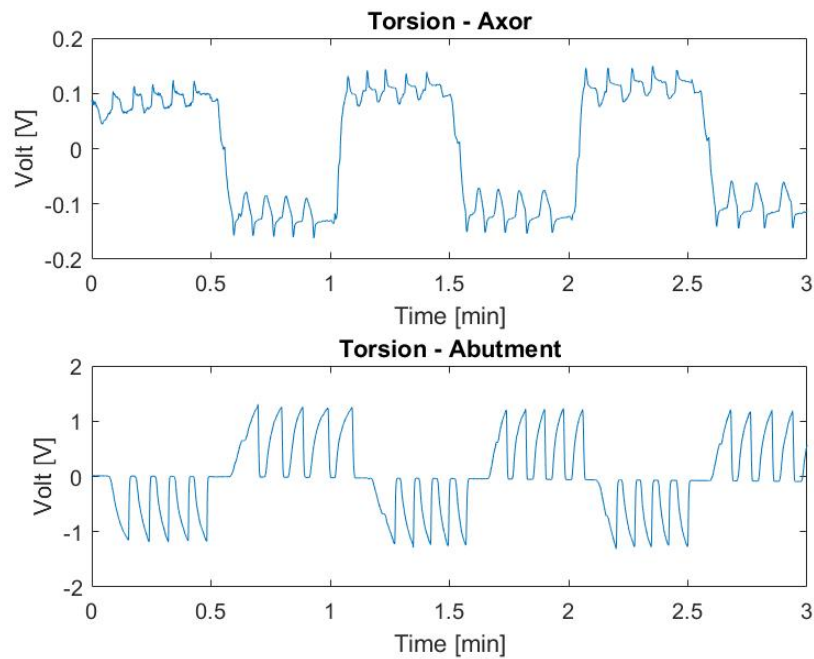


Figure 39: Torsional moment measured by the Axor and abutment.

6.2.3 Comparison Test

Bending moment:

The comparison between the Axor and iPecs can be seen in Figures 40 and 41, whereas the comparison between the abutment and iPecs can be seen in Figures 42 and 43. The y axis represents Newton-meters and the x axis time.

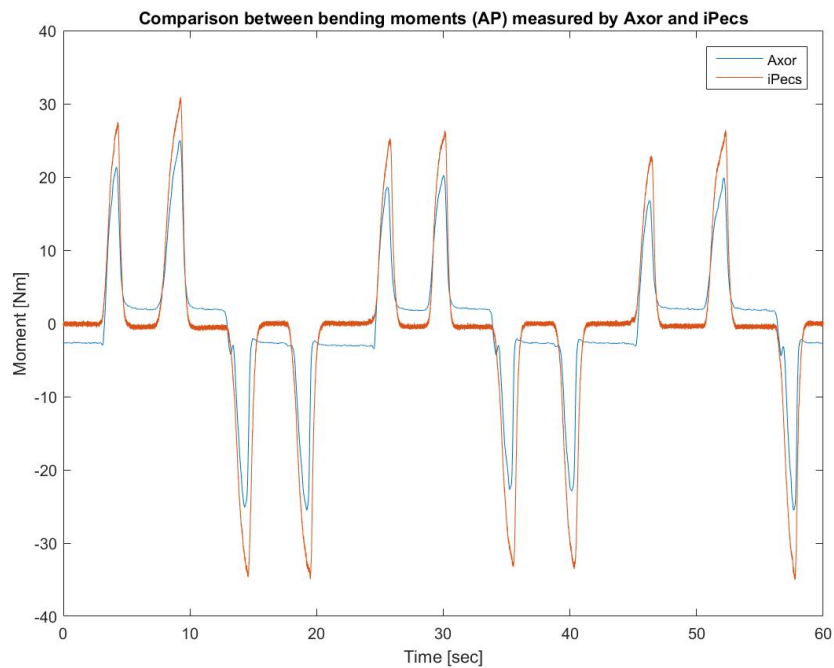


Figure 40: Comparison between bending moments around the AP axis, measured by the Axor and iPecs.

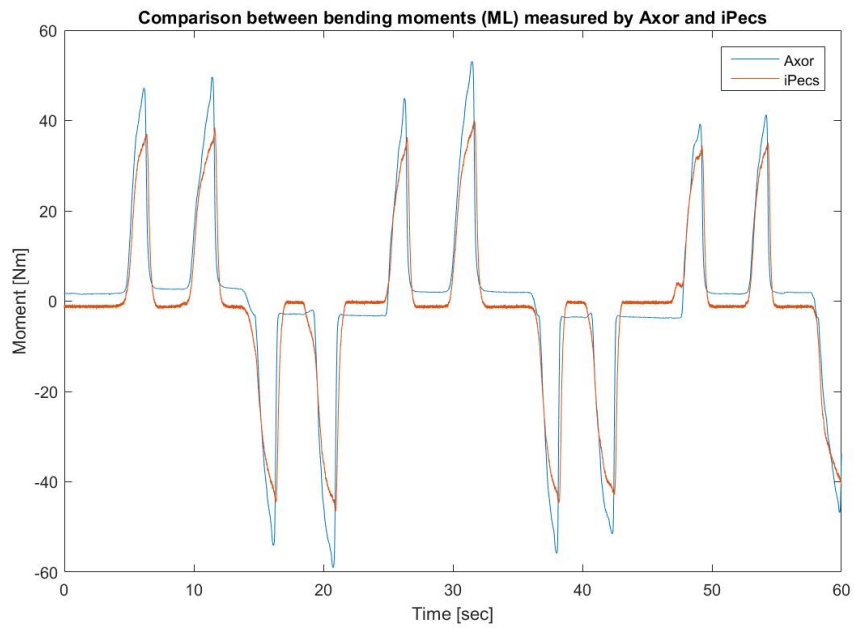


Figure 41: Comparison between bending moments around the ML axis, measured by the Axor and iPecs.

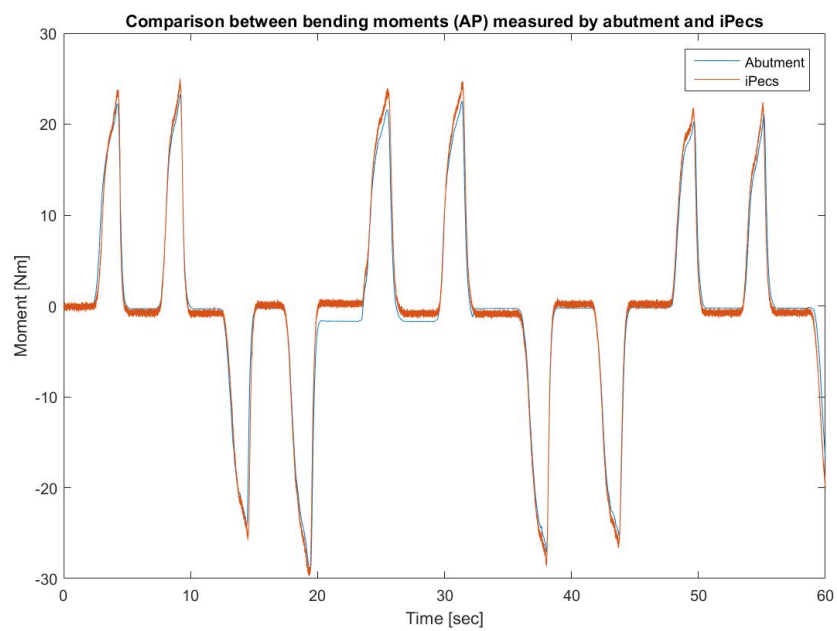


Figure 42: Comparison between bending moments around the AP axis, measured by the abutment and iPecs.

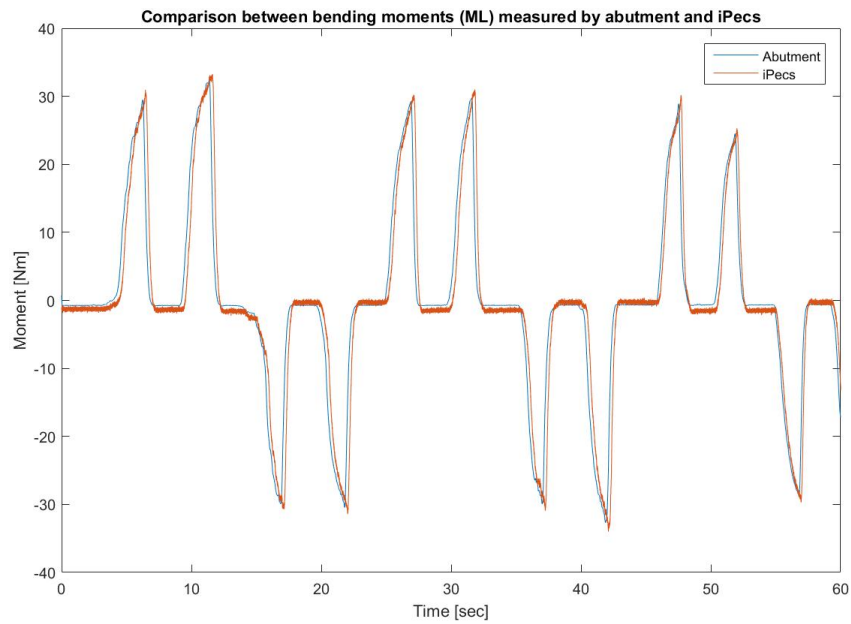


Figure 43: Comparison between bending moments around the ML axis, measured by the abutment and iPecs.

Torsional moment:

The comparison between the Axor and iPecs can be seen in Figure 44, whereas the comparison between the abutment and iPecs can be seen in Figure 45. The y axis represents Newton-meters and the x axis time.

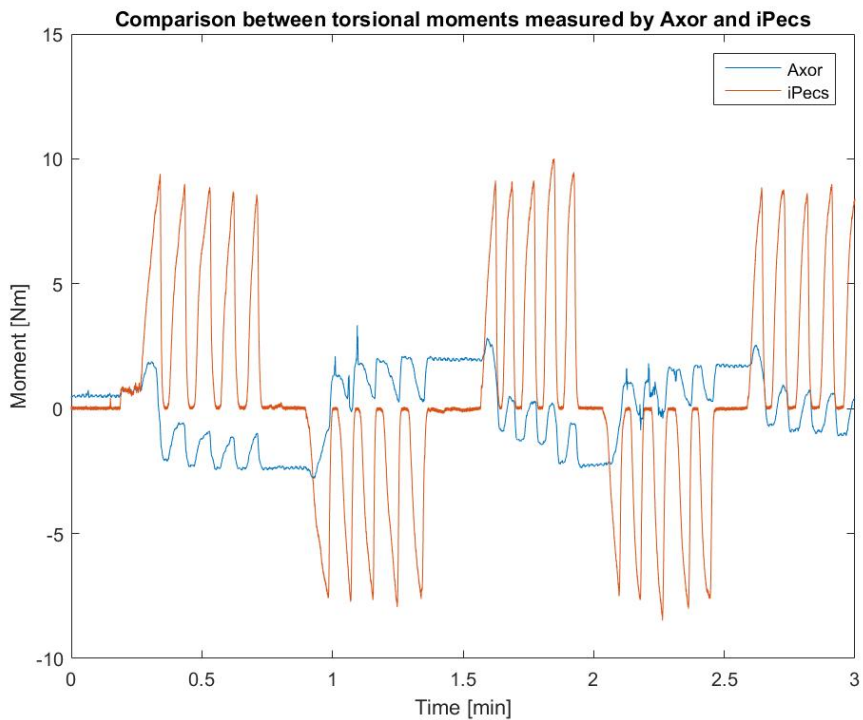


Figure 44: Comparison between torsional moments measured by the Axor and iPecs.

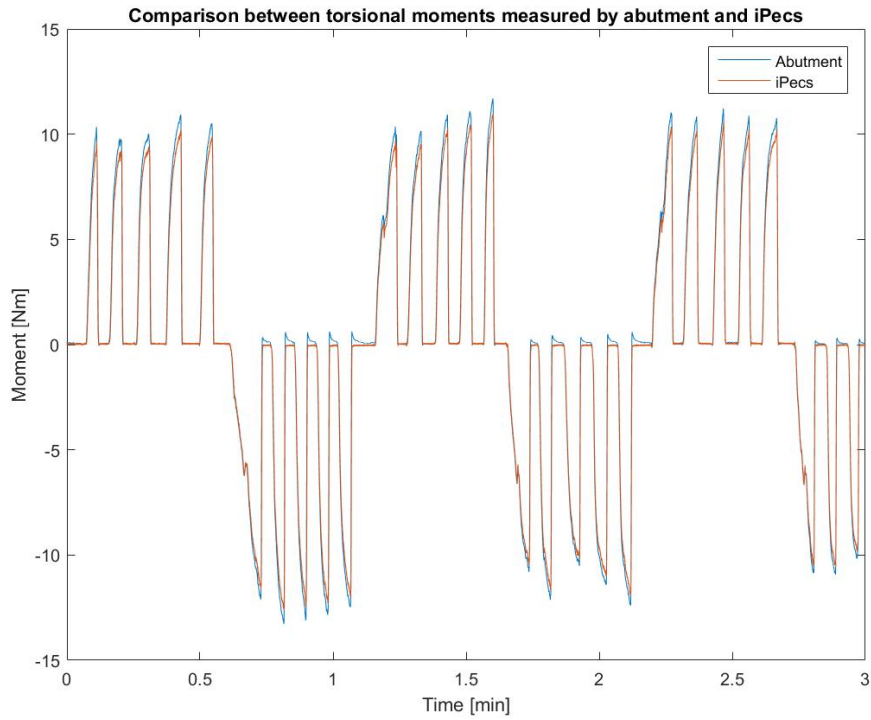


Figure 45: Comparison between torsional moments measured by the abutment and iPecs.

Axial force:

Figure 46 shows the comparison between the axial force measured by the abutment and iPecs. The y axis represents Newtons and the x axis time.

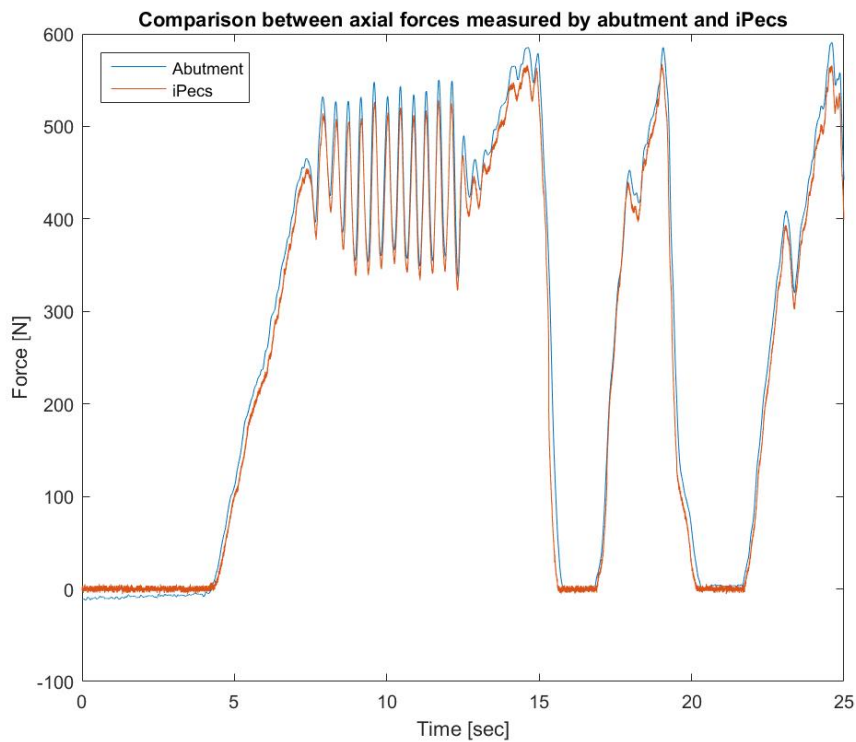


Figure 46: Comparison between axial forces measured by the abutment and iPecs.

6.2.4 SD Card Communication

Figure 47 shows the comparison between real time communication and SD card communication, where volts are plotted against samples.

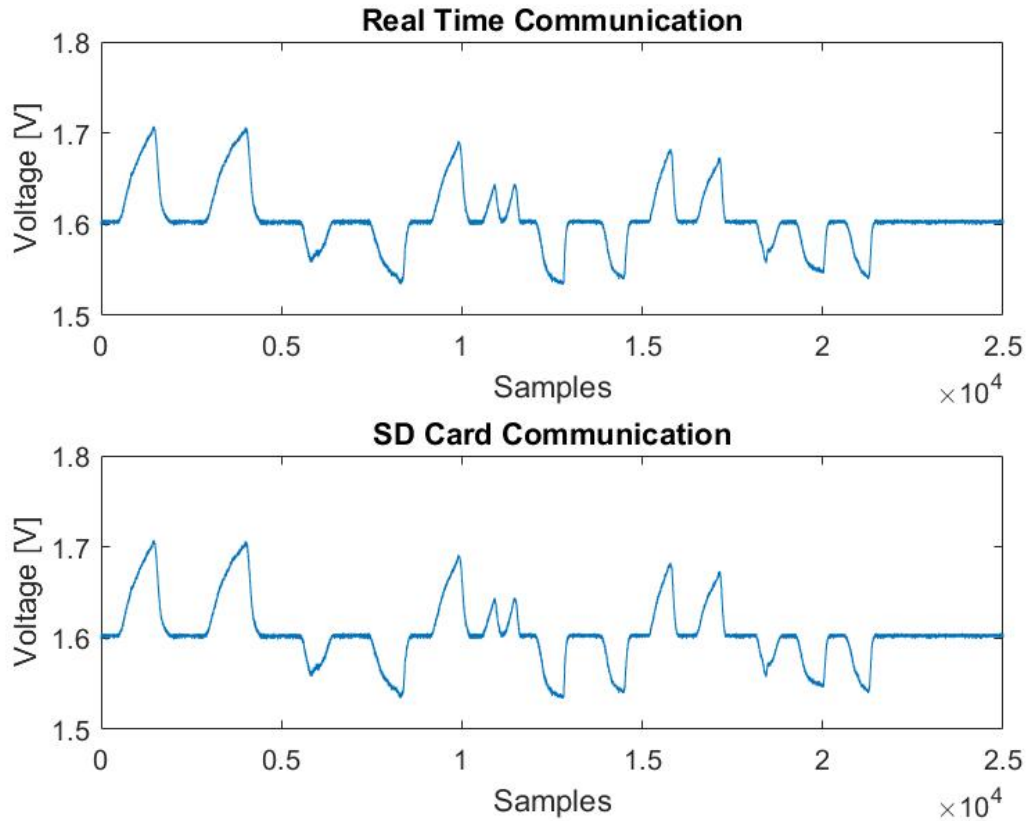


Figure 47: Comparison between real time and SD card communication.

6.3 Patient Pilot

Walking back and forth:

Figure 48 shows 40 seconds of the recording session when the patient was asked to walk back and forth on a normal pace, where Newton-meters are plotted against time. During the first twenty seconds, the patient walked on a normal pace, then stopped for approximately 7 seconds, and finally turned around and walked back for about 13 seconds.

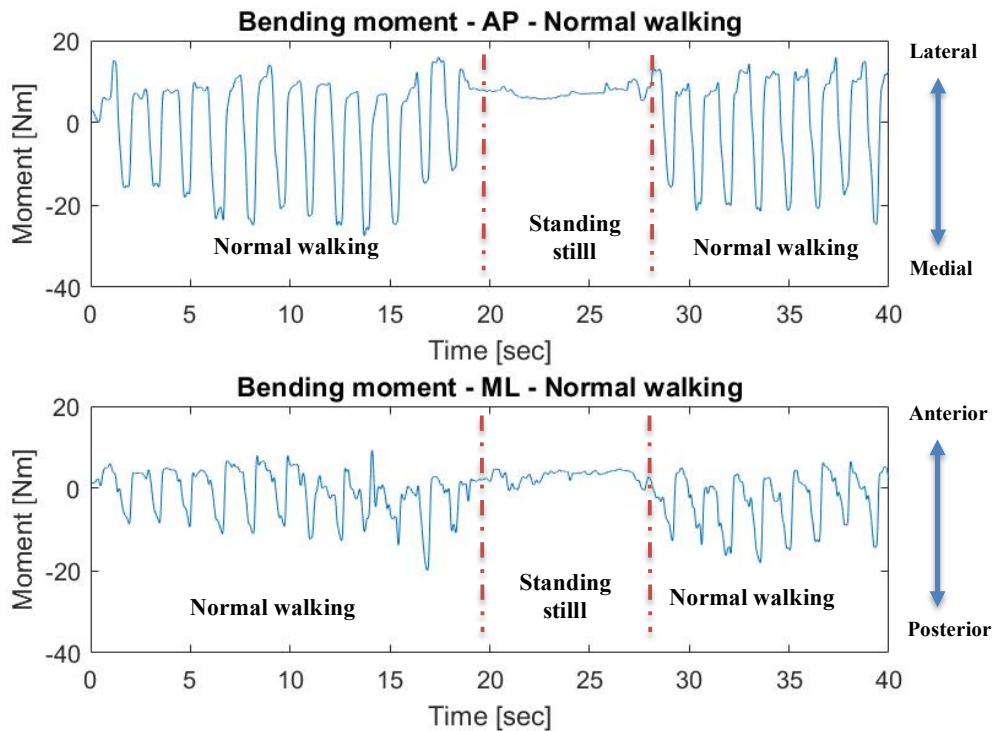


Figure 48: Bending moments measured during normal walking, both around the anteroposterior (AP) and mediolateral (ML) axis.

Sitting down and standing up:

Figure 49 shows 20 seconds of the patient sitting down and standing up alternately (4x standing up and 3x sitting down), where Newton-meters are plotted against time.

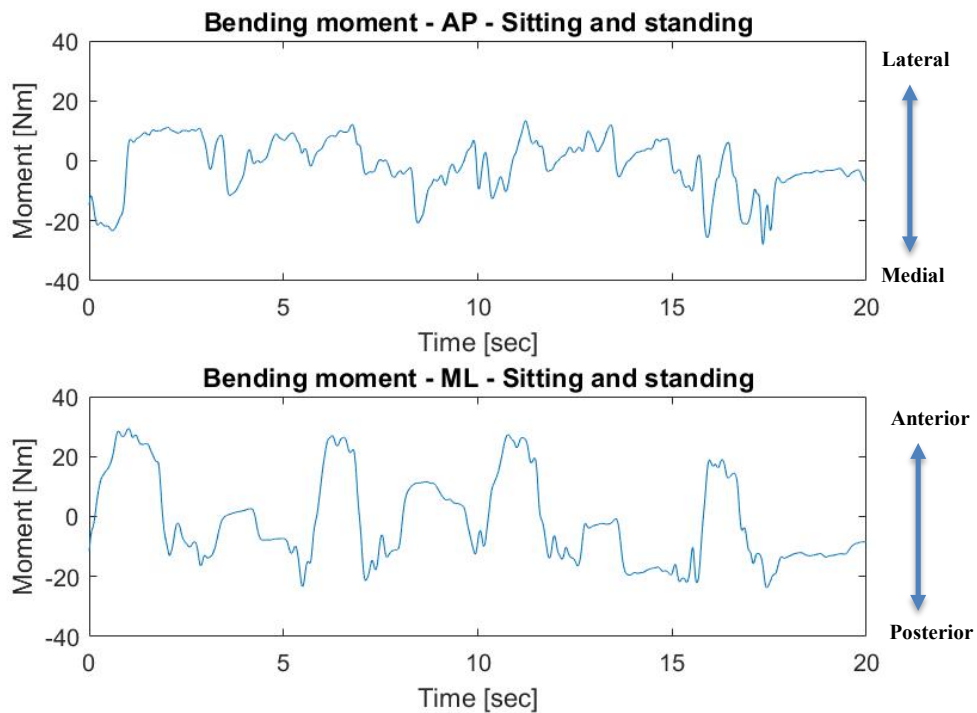


Figure 49: Bending moments measured, both around the anteroposterior (AP) and mediolateral (ML) axis, when the patient sat down and stood up alternately.

Maximum voluntary load applied in the AP direction:

The following graphs show the results when the patient applied as much voluntary load to the abutment in 1) the posterior direction, see Figure 50, and 2) the anterior direction, see Figure 51. The y axis represents Newton-meters and the x axis time.

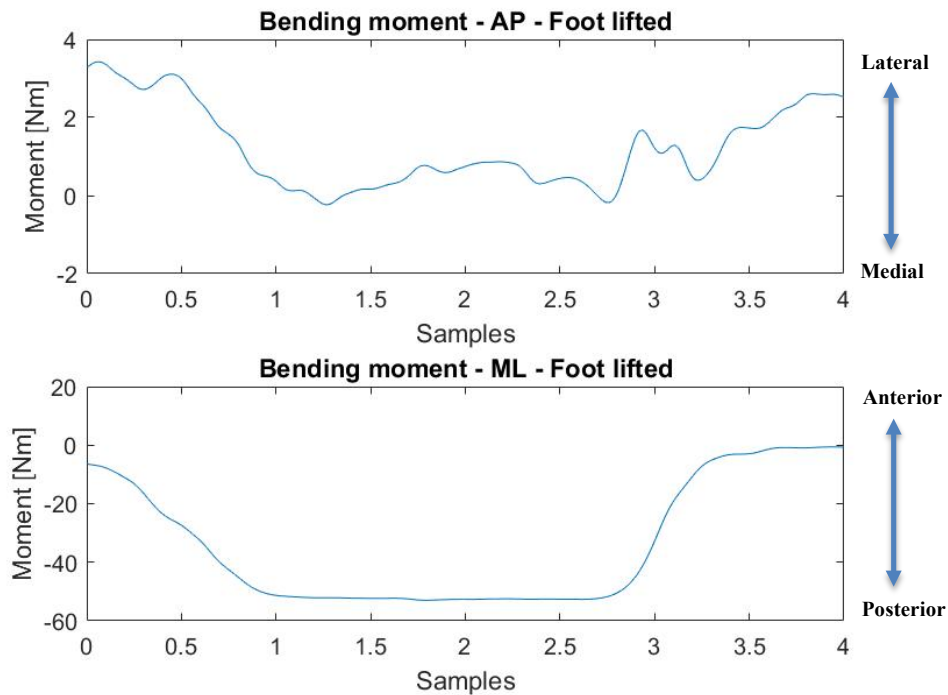


Figure 50: Bending moments measured, both around the anteroposterior (AP) and mediolateral (ML) axis, when maximum voluntary load is applied in the posterior direction.

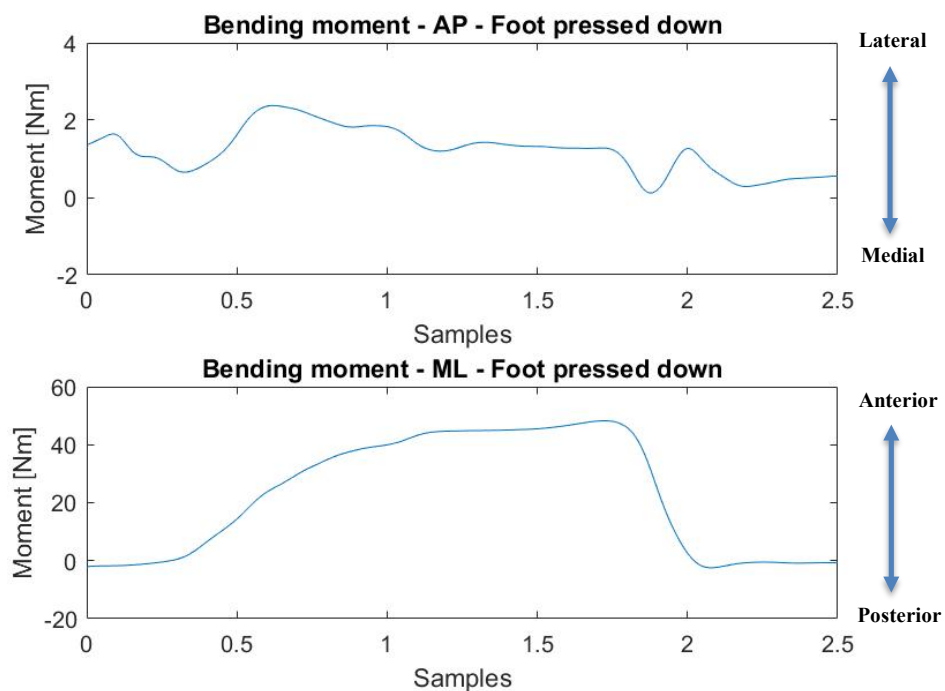


Figure 51: Bending moments measured, both around the anteroposterior (AP) and mediolateral (ML) axis, when maximum voluntary load is applied in the anterior direction.

7 Discussion

7.1 Testing

7.1.1 Selecting Appropriate Gain Resistances

The fact that no signal was obtained when measuring axial force can be explained by the selected placement of the strain gauges within the Axor. The conical cylinder which the strain gauges are attached to, does not seem to compress/stretch enough to see a signal when axial force is applied to the abutment fitted inside the Axor, i.e. the force does not fully transfer to the cylinder.

If a small portion of the axial force is being transferred to the cylinder, it should be possible to apply signal treatment and processing techniques to denoise the signal of interest. However, due to the fact that the offset nulling in the current PCB can not be performed by hardware (using a potentiometer), the gain of the amplifier measuring axial force could not be selected high enough (without saturating) to see a signal.

The way the axial force was applied in the test was very un-precise, as a person was asked to jump lightly on the Axor in hope of applying approximately 1200 N to it. An alternative way would have been to ask the person applying the load (weighing 90 kg), to hold a weight of 30 kg, thus resulting in 120 kg (1200 N) being applied to the Axor. A more precise way would have been to test the axial force in a MTS machine, which can apply axial force with high precision.

7.1.2 Calibration Test

Bending moment:

As can be seen from Figures 35 and 36, the profiles of the signals obtained from the Axor and abutment are very similar, which made the calibration easy. The fact that the calibrated Axor data were so similar to the abutment data, see Figures 37 and 38, indicates that the linear model obtained was accurate. However, if examined closely, it can be seen that the baseline for the Axor changes slightly after the bending direction is switched. The fact that silicone glue was applied on top of the whole strain gauge installation, thus decreasing the clearance around the strain gauge, could be contributing to this small baseline shift.

Torsional moment:

As noted before, the two signals recorded from the Axor and abutment were very different, thus making the calibration impossible. The difference mainly lies in the large baseline shift seen in the Axor signal, and the signal overshoot when torque is released. The baseline shift can be explained by an apparent latching of the Axor during directional changes. Also, the small clearance around the strain gauges could be contributing to this shift as well. The cause for the signal overshoot, however, is not fully understood.

7.1.3 Comparison Test

Bending moment:

The comparison between the Axor and the iPecs, see Figures 40 and 41, indicates that the profile of the signals are similar, with the exception that the baseline for the Axor changes each time the bending direction is switched (alternates between -2 Nm and 2 Nm approximately). The intensity of the bending moments around the AP axis, when the shifted baseline is considered as reference, are not identical to the iPecs, i.e. the peak moments in the Axor appear to be approximately 40% lower than in the iPecs. However, for the bending moments around the ML axis, the intensity seems to be the same (when the shifted baseline is considered as reference). Like pointed out before, the small clearance around the strain gauges is probably contributing to this baseline shift where friction comes into play. The fact that the intensity of the bending moment around the ML axis is so similar to the iPecs, indicates that the load applied to the abutment is being fully transferred to the conical cylinder inside the Axor. Therefore, it was surprising to see that the results for the bending moment around the AP axis were different. A possible explanation could be that the mounting process of the strain gauges (measuring AP bending moments) was compromised.

The comparison between the abutment and iPecs, see Figures 42 and 43, demonstrates that the measured signals are almost identical, i.e. the baseline stays approximately the same and the peak moments measured are equivalent. The fact that the two signals were so similar clearly demonstrates that the unit conversion was accurate and reliable. It also emphasizes that in order to get a reliable signal, the strain gauges need to have clearance (like the strain gauges mounted on the abutment), in order to ensure that no physical objects are interfering with the strain gauges and consequently changing the signal.

Torsion:

When comparing the torsion signals obtained from the Axor and iPecs, see Figure 44, it can be seen that the signal profiles are very different, mainly due to the baseline shift seen in the Axor signal. The intensities of the signals are also not identical, i.e. the peak moment measured by the iPecs is approximately 10 times higher than the peak moment measured by the Axor, which indicates that the applied torque does not fully transfer to the part inside the Axor where the strain gauges are mounted. The fact that the Axor signal did not overshoot after torque was released was surprising since the results from the calibration test demonstrated that. Therefore, a side test was conducted where the torsional moment applied to the abutment was increased incrementally, while measuring from the Axor. Torque was applied 12 times to the abutment (in each direction) - 5 Nm (3x), 10 Nm (3x), 15 Nm (3x) and 20 Nm (3x) respectively. The results can be seen in Figure 52 which indicates that an interference with the signal is detected with higher torque. This explains why the results in the comparison test were different from the results in the calibration test, since the torque applied in the comparison test was usually under 10 Nm, but around 20 Nm in the calibration test. Why the signal overshoot appears only when higher torque is applied to the device is still hard to explain, but one might argue that a mechanical deformation at the interface where the strain gauges are mounted is occurring.

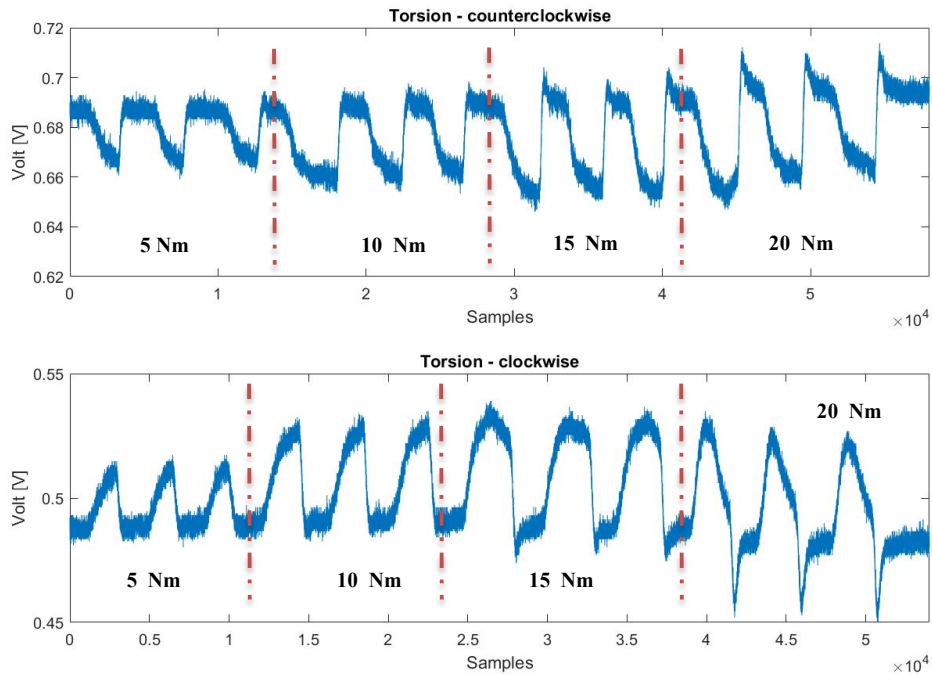


Figure 52: Torsional moments measured by the Axor – Side test.

The comparison between the abutment and iPecs, see Figure 45, demonstrates however that the curves for both signals are identical (like for the bending moments). Like previously mentioned, this indicates that the unit conversion was reliable and that clearance around the strain gauges is important.

Axial force:

The signals obtained from the abutment and iPecs are almost identical, i.e. the baseline stays approximately the same and the forces being measured are similar (abutment results a bit higher), which again verifies that the unit conversion was accurate and that clearance around the strain gauges is essential.

7.1.4 SD Card Communication

The comparison between real time communication and SD card communication demonstrated that the two communication modules were equivalent and confirmed that the SD card communication is reliable.

7.2 Patient Pilot

The fact that bending moments were successfully recorded in a patient during ambulation verified the functionality of the designed electronics and acquisition algorithms.

Walking back and forth:

As can be seen from the results, there were approximately 20 gait cycles recorded. The obtained bending moments during normal walking are found to be in the correct order of magnitude, but a bit on the lower side when compared to available studies [19][24][27][48]. A possible explanation could be that the patient was cautious as this

was his first time testing the instrumented device, and therefore did not apply full load. The fact that the bending moments around the AP axis were found to be higher than the bending moments around the ML axis, was surprising as available studies usually indicate the opposite. This can however be explained by the subject-to-subject variability in the loading scenario.

Sitting down and standing up:

The bending moments around the ML axis show a clear trend when the patient sat down and stood up alternately, which reveals that higher bending moments are applied to the abutment when the patient stands up compared to when he sits down. However, the bending moments around the AP axis are random, and no clear trend is observed for the sitting and standing regime.

Maximum voluntary load applied in the AP direction:

The obtained results when the patient applied maximum voluntary load to the abutment reveal that the bending moment around the AP axis is almost negligible (ranging between a few Newton-meters) and the maximum moments around the ML axis is approximately ± 50 Nm. This was to be expected since the patient applied the load in the AP direction thus inducing a large change in resistance on the strain gauges positioned in that plane.

7.3 Updated design

After having conducted the tests, the design of the PCB was updated to alleviate some of the problems that emerged, see Figure 53. In the updated design, two channels were added to the PCB, i.e. one measuring axial force, and one measuring torsion. This resulted in a new PCB having 7 channels – 3 for bending, 2 for axial force and 2 for torsion. The reason to add those channels was to allow for the calibration test (applies only to the axial force and torsion) to be conducted in a more efficient way. By adding the channels, the test would not have to be conducted separately where the gain resistances are changed between runs, and therefore give a more accurate results. In addition to adding the two channels, potentiometers were added to each Wheatstone bridge, thus allowing for the offset nulling to be conducted by hardware and consequently prevent the dynamic range of the measurement to be restricted. Due to time restriction, the updated PCB could not be tested within this thesis work.

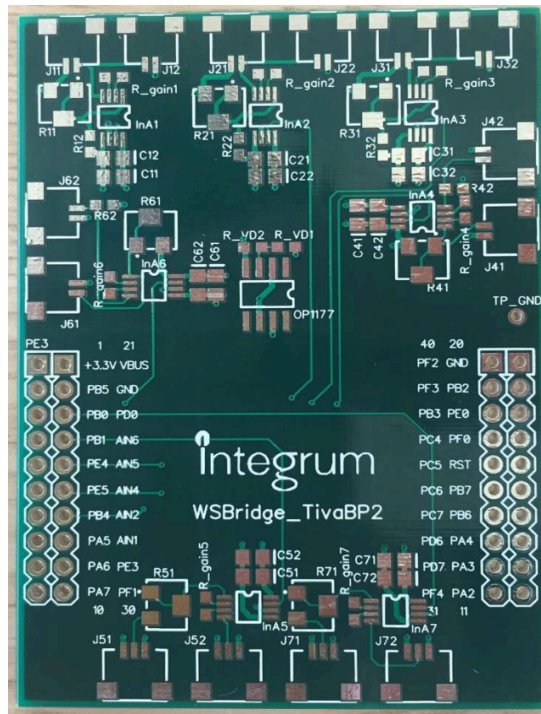


Figure 53: The updated PCB.

7.4 Future Work

Due to the fact that the instrumented Axor could not measure axial force, the placement of strain gauges would need to be revised, and a force distribution simulation conducted prior to the implementation. The same goes for the strain gauges measuring torsion due to the deformed signal profile and low signal intensity.

The drawbacks associated with the baseline shift seen in signals when measuring bending should also be addressed. Signal processing techniques could be used in the future to compensate for the shift. An alternative way would be to implement an algorithm where the reference value indicating no strain, would get updated depending on the bending direction.

Since the silicone glue mounted on top of the strain gauge installation seems to be contributing to the baseline shift seen in the signals, it might be a good next step to use strain gauges with external solder terminals to increase clearance inside the Axor and mitigate friction.

Although the acquisition system designed in this project is functioning, it has drawbacks since it was designed to only sample at a predefined frequency. An adaptive acquisition system where the sampling frequency changes depending on the activity of the user would be optimal, since it ensures that important information will not be missed, and limits the amount of information being stored. A high sampling frequency would be set when the patient is involved in a high impact activity, but a low sampling frequency set otherwise. One way to implement this kind of adaptive system would be to add an accelerometer to the system. The accelerometer would detect abrupt changes in acceleration, like for instance during a fall, so the microcontroller could be programmed in such a way that the sampling frequency

increases/decreases depending on the status of the accelerometer. Another way to implement this would be to take the average value of several samples, and change the sampling frequency depending on the standard deviation calculated. If the standard deviation reaches a predefined threshold, indicating that the patient is involved in a high-impact activity (such as a fall), the system should increase the sampling frequency to make sure important information will not be missed.

Once the issues mentioned above have been solved, the instrumented Axor could be taken to the next level by adding e.g. motion sensors and pattern recognition algorithms in order to categorize activities and link them to applied loads on the implant. Warning features, such as sound or vibration, could also be beneficial by informing patients when they are involved in high stress activities. Adding a Global Positioning System (GPS) or a step counter to the system could also be practical since it would allow the patient to monitor the distance travelled and the step count. These are just examples of what could be done in the future to enhance the system even further, but in the world of smart technology the possibilities are limitless.

8 Conclusion

The obtained results imply that the axial force could not be measured from the selected location of the strain gauges within the Axor. Torsional moments measured from the Axor were also challenging, due to friction and/or an apparent latching during directional changes thus inducing a shift in the baseline. A signal overshoot was detected with increased torque which can be explained by a mechanical deformation at the interface where the strain gauges are mounted. As a result, the selected placement of the strain gauges for both the axial force and torque needs to be revised. The results for the measured bending moments were reliable and found to be similar to those obtained with a commercially available 6-axis transducer. Bending moments were also successfully recorded in a patient during ambulation, thus verifying the functionality of the designed electronics, acquisition algorithms and communication modules.

This thesis has been a stepping stone in the development of a functional monitoring device for osseointegrated transfemoral prostheses. The feasibility of the concept has been demonstrated, but further work is needed before this technology can be used in activities of the daily living.

9 References

- [1] M. R. Pitkin, “Lower Limb Prosthesis,” in *Biomechanics of Lower Limb Prosthetics*, Springer Berlin Heidelberg, 2010, pp. 1–27.
- [2] M. Zhang, A. F. T. Mak, and V. C. Roberts, “Finite element modelling of a residual lower-limb in a prosthetic socket: a survey of the development in the first decade,” *Med. Eng. Phys.*, vol. 20, no. 5, pp. 360–373, Jul. 1998.
- [3] G. K. Klute, J. S. Berge, W. Biggs, S. Pongnumkul, Z. Popovic, and B. Curless, “Vacuum-Assisted Socket Suspension Compared With Pin Suspension for Lower Extremity Amputees: Effect on Fit, Activity, and Limb Volume,” *Arch. Phys. Med. Rehabil.*, vol. 92, no. 10, pp. 1570–1575, Oct. 2011.
- [4] M. Zhang, A. R. Turner-Smith, V. C. Roberts, and A. Tanner, “Frictional action at lower limb/prosthetic socket interface,” *Med. Eng. Phys.*, vol. 18, no. 3, pp. 207–214, Apr. 1996.
- [5] K. Hagberg and R. Brånemark, “Consequences of non-vascular trans-femoral amputation: A survey of quality of life, prosthetic use and problems,” *Prosthet. Orthot. Int.*, vol. 25, no. 3, pp. 186–194, Dec. 2001.
- [6] D. K. Hagberg, E. Häggström, M. Uden, and R. Brånemark, “Socket versus bone-anchored trans-femoral prostheses: Hip range of motion and sitting comfort,” *Prosthet. Orthot. Int.*, vol. 29, no. 2, pp. 153–163, Jan. 2005.
- [7] K. Hagberg and R. Brånemark, “One hundred patients treated with osseointegrated transfemoral amputation prostheses—rehabilitation perspective,” *J. Rehabil. Res. Dev.*, vol. 46, no. 3, pp. 331–344, 2009.
- [8] R. Branemark, P. I. Branemark, B. Rydevik, and R. R. Myers, “Osseointegration in skeletal reconstruction and rehabilitation: A review,” *Dep. Veterans Aff.*, vol. 38, no. 2, pp. 175–181, Apr. 2001.
- [9] R. Brånemark, Ö. Berlin, K. Hagberg, P. Bergh, B. Gunterberg, and B. Rydevik, “A novel osseointegrated percutaneous prosthetic system for the treatment of patients with transfemoral amputation,” *Bone Jt. J*, vol. 96-B, no. 1, pp. 106–113, Jan. 2014.
- [10] J. Sullivan, M. Uden, K. P. Robinson, and S. Sooriakumaran, “Rehabilitation of the trans-femoral amputee with an osseointegrated prosthesis: The United Kingdom experience,” *Prosthet. Orthot. Int.*, vol. 27, no. 2, pp. 114–120, Aug. 2003.
- [11] “OPRA Implant System,” *Integrum*. [Online]. Available: <http://www.integrum.se/index.php/opra-implant-system>. [Accessed: 03-Feb-2016].
- [12] L. Kumar, B. P. Singh, J. Rao, and K. Singh, “Osseoperception in Implants Supported Prosthesis-A,” *Online J. Med. Med. Sci. Res.*, vol. 1, no. 1, pp. 1–4, 2012.
- [13] Integrum, “OPRA Axor II - Instructions for Use.” [Brochure], (n.d.).
- [14] K. Bregler, “Instrumentation of a Safety Device for Lower Limb Prosthesis,” Karlsruhe Institute of Technology, Germany, 2016.
- [15] A. Muro-de-la-Herran, B. Garcia-Zapirain, and A. Mendez-Zorrilla, “Gait Analysis Methods: An Overview of Wearable and Non-Wearable Systems, Highlighting Clinical Applications,” *Sensors*, vol. 14, no. 2, pp. 3362–3394, Feb. 2014.
- [16] L. Ren, R. K. Jones, and D. Howard, “Whole body inverse dynamics over a complete gait cycle based only on measured kinematics,” *J. Biomech.*, vol. 41, no. 12, pp. 2750–2759, Aug. 2008.

- [17] L. Frossard, J. Beck, M. Dillon, and J. Evans, "Development and preliminary testing of a device for the direct measurement of forces and moments in the prosthetic limb of transfemoral amputees during activities of daily living," *JPO J. Prosthet. Orthot.*, vol. 15, no. 4, pp. 135–142, 2003.
- [18] S. R. Simon, "Quantification of human motion: gait analysis—benefits and limitations to its application to clinical problems," *J. Biomech.*, vol. 37, no. 12, pp. 1869–1880, Dec. 2004.
- [19] W. C. C. Lee, L. A. Frossard, K. Hagberg, E. Haggstrom, D. L. Gow, S. Gray, and R. Brånemark, "Magnitude and variability of loading on the osseointegrated implant of transfemoral amputees during walking," *Med. Eng. Phys.*, vol. 30, no. 7, pp. 825–833, Sep. 2008.
- [20] S. J. M. Bamberg, A. Y. Benbasat, D. M. Scarborough, D. E. Krebs, and J. A. Paradiso, "Gait Analysis Using a Shoe-Integrated Wireless Sensor System," *IEEE Trans. Inf. Technol. Biomed.*, vol. 12, no. 4, pp. 413–423, Jul. 2008.
- [21] S. R. Koehler, Y. Y. Dhaher, and A. H. Hansen, "Cross-validation of a portable, six-degree-of-freedom load cell for use in lower-limb prosthetics research," *J. Biomech.*, vol. 47, no. 6, pp. 1542–1547, Apr. 2014.
- [22] L. Frossard, D. L. Gow, K. Hagberg, N. Cairns, B. Contoyannis, S. Gray, R. Brånemark, and M. Percy, "Apparatus for monitoring load bearing rehabilitation exercises of a transfemoral amputee fitted with an osseointegrated fixation: A proof-of-concept study," *Gait Posture*, vol. 31, no. 2, pp. 223–228, Feb. 2010.
- [23] L. Frossard, N. Stevenson, J. Smeathers, E. Häggström, K. Hagberg, J. Sullivan, D. Ewins, D. L. Gow, S. Gray, and R. Brånemark, "Monitoring of the load regime applied on the osseointegrated fixation of a trans-femoral amputee: A tool for evidence-based practice," *Prosthet. Orthot. Int.*, vol. 32, no. 1, pp. 68–78, Jan. 2008.
- [24] L. Frossard, D. Lee Gow, B. Contoyannis, A. Nunn, and R. Brånemark, "Load applied on the abutment of transfemoral amputees fitted with an osseointegrated implant during load bearing exercises using a long pylon," *Int. Soc. Prosthet. Orthot.*, pp. 55–56, 2004.
- [25] L. A. Frossard, R. Tranberg, E. Haggstrom, M. Percy, and R. Brånemark, "Load on osseointegrated fixation of a transfemoral amputee during a fall: Loading, descent, impact and recovery analysis," *Prosthet. Orthot. Int.*, vol. 34, no. 1, pp. 85–97, Mar. 2010.
- [26] L. A. Frossard, "Load on osseointegrated fixation of a transfemoral amputee during a fall: Determination of the time and duration of descent," *Prosthet. Orthot. Int.*, vol. 34, no. 4, pp. 472–487, Dec. 2010.
- [27] L. A. Frossard, E. Haggstrom, K. Hagberg, and R. Brånemark, "Load applied on a bone-anchored transfemoral prosthesis: characterisation of a prosthesis : a pilot study," *J. Rehabil. Res. Dev.*, vol. 50, no. 5, pp. 619–634, 2013.
- [28] "Nasa Tech Brief Announced iPecs as Winner," *College Park*. [Online]. Available: <http://www.college-park.com/company/news/61-company/news/151-nasa-tech-brief-announced-ipecs-as-winner>. [Accessed: 05-Feb-2016].
- [29] "iPecs Lab - Wireless Gait Lab," *College Park*. [Online]. Available: <http://www.college-park.com/images/pdf/cpi-specs-ipeclab.pdf>. [Accessed: 05-Feb-2016].
- [30] J. Fraden, *Handbook of Modern Sensors: Physics, Design, and Applications*. Springer New York, 2010.
- [31] K. Hoffmann, "An introduction to stress analysis and transducer design using strain gauges," *HBM Test Meas.*, 2012.

- [32] “How Is Temperature Affecting Your Strain Measurement Accuracy?,” *National Instruments*. [Online]. Available: <http://www.ni.com/white-paper/3432/en/>. [Accessed: 16-Feb-2016].
- [33] “Strain Gauge,” *Wikipedia*. [Online]. Available: https://en.wikipedia.org/wiki/Strain_gauge. [Accessed: 16-Feb-2016].
- [34] “Strain gauge connections and bridge circuits,” *Tokyo Sokki Kenkyujo Co., Ltd.* [Online]. Available: http://www.tml.jp/e/product/strain_gauge/bridge_list.html. [Accessed: 27-Mar-2016].
- [35] “Strain Gauge Configuration Types,” *National Instruments*. [Online]. Available: <http://www.ni.com/white-paper/4172/en/#toc5>. [Accessed: 23-Mar-2016].
- [36] “Measuring Strain with Strain Gages,” *National Instruments*. [Online]. Available: <http://www.ni.com/white-paper/3642/en/>. [Accessed: 27-Mar-2016].
- [37] “Anatomical terms of location,” *Wikipedia, the free encyclopedia*. 09-May-2016.
- [38] J. Boersch, “How to install a strain gauge with an adhesive | HBM,” *HBM - Measure and Predict with Confidence*. [Online]. Available: <http://www.hbm.com/en/4637/install-strain-gauge-with-adhesive>. [Accessed: 11-May-2016].
- [39] “Tiva™ TM4C123GH6PM Microcontroller,” *Texas Instruments*, 2014. [Online]. Available: <http://www.ti.com/lit/ds/symlink/tm4c123gh6pm.pdf>. [Accessed: 05-May-2016].
- [40] “Tiva C Series TM4C123G LaunchPad (EK-TM4C123GXL).” [Online]. Available: <http://www.ti.com/ww/en/launchpad/launchpads-connected-ek-tm4c123gxl.html>. [Accessed: 05-May-2016].
- [41] “MICROSD BOOSTERPACK,” *BoardZoo.com*. [Online]. Available: <http://boardzoo.com/index.php/microsd-boosterpack.html#.VysV8hV945s>. [Accessed: 05-May-2016].
- [42] Maitra and L. V. Prasad, *Handbook of Mechanical Design*. Tata McGraw-Hill Education, 1995.
- [43] “Mathematics for Engineering - Basic Algebra,” *Freestudy - Free Tutorials on Engineering and Science*. [Online]. Available: <http://www.freestudy.co.uk/maths/algebra4.pdf>. [Accessed: 05-Apr-2016].
- [44] “Wide Supply Range, Rail-to-Rail Output Instrumentation Amplifier - AD8226,” *Mouser Electronics*. [Online]. Available: <http://www.mouser.com/ds/2/609/AD8226-877720.pdf>. [Accessed: 05-May-2016].
- [45] “TPS736xx Cap-Free, NMOS, 400-mA Low-Dropout Regulator with Reverse Current Protection,” *Texas Instruments*, 2015. [Online]. Available: <http://www.ti.com/lit/ds/sbvs038u/sbvs038u.pdf>. [Accessed: 05-May-2016].
- [46] “TIMET TIMETAL® 6-4 ELI Titanium Alloy (Ti-6Al-4V ELI; ASTM Grade 23) (Solution Treated; 0.025 - 1.000 in Sheet and Plate; Per ASTM B265),” *MatWeb Material Property Data*. [Online]. Available: <http://www.matweb.com/search/DataSheet.aspx?MatGUID=3e9ab476890947859e7a33f04ef71713>. [Accessed: 05-May-2016].
- [47] “AK Steel 301 Austenitic Stainless steel,” *MatWeb Material Property Data*. [Online]. Available: <http://www.matweb.com/search/datasheet.aspx?matguid=7ab1936975fd4cb2937286a8a004e052>. [Accessed: 05-May-2016].
- [48] L. Frossard, K. Hagberg, E. Haggstrom, and R. Branemark, “Load-Relief of Walking Aids on Osseointegrated Fixation: Instrument for Evidence-Based

Practice,” *IEEE Trans. Neural Syst. Rehabil. Eng.*, vol. 17, no. 1, pp. 9–14, Feb. 2009.